Received: 31 December 2022 | Accepted: 1 August 2023

DOI: 10.1002/fut.22457

RESEARCH ARTICLE

THE JOURNAL OF FUTURES MARKETS WILEY

Estimation of rare disaster concerns from option prices—An arbitrage-free RND-based smile construction approach

Pascal Albert[1] | **Michael Herold**[2*] | **Matthias Muck**[1]

[1]Chair of Banking and Financial Control, University of Bamberg, Bamberg, Germany

[2]ZF Group, Friedrichshafen, Germany

Correspondence
Pascal Albert, Chair of Banking and Financial Control, University of Bamberg, 96045 Bamberg, Germany.
Email: pascal.albert@uni-bamberg.de

Abstract

This research addresses the estimation of measures of rare disaster concerns from option prices. We propose a new smile construction approach to obtain the required continuum of implied volatilities from discretely sampled observations that are affected by microstructure noise. We extrapolate implied volatilities of far out-of-the-money options by modeling the tails of the risk-neutral return distribution (RND) ensuring that option prices do not admit arbitrage. Our numerical analysis and empirical application show that the RND-based approach consistently outperforms standard techniques. It substantially reduces estimation errors resulting in considerably higher estimates of the rare disaster concern index ($\mathbb{RIX}$) when event risk is high.

KEYWORDS

microstructure noise, numerical errors, option-implied risk measures, rare disaster concerns, volatility smile construction

JEL CLASSIFICATION

C14, G10, G13, G17

1 | INTRODUCTION

In the recent macrofinance literature, rare disaster risk is considered to explain the equity premium puzzle. Barro (2006, 2009) obtains realistic equity risk premiums by adding disaster risk to the consumption process assuming that the probability for rare disasters is constant. Stock returns are i.i.d. in this model. A caveat of this approach is that stock volatility is too low. To obtain realistic stock volatilities, Wachter (2013) extends this model assuming stochastic disaster probabilities and recursive preferences.[1]

*This study was written during the author's previous employment at the University of Bamberg, Chair of Banking and Financial Control, 96045 Bamberg, Germany. All views, thoughts, and opinions expressed are solely those of the author and do not necessarily reflect the views and positions of ZF or any associated entities.

[1]In fact, Wachter (2013) assumes the special case in which the elasticity of intertemporal substitution is equal to 1. These preferences can be interpreted as Cobb–Douglas preferences.

Disaster risk is also reflected in option prices. Among other things, this is highlighted by the establishment of the Chicago Board Options Exchange (CBOE) skewness (SKEW) index derived from the implied volatility skew of S&P 500 options.[2] Therefore, option prices can be used to estimate the (latent) amount of jump risk and thus reveal important information on the current risk assessment of the market. Gao et al. (2018, 2019) propose the rare disaster concern risk index $\mathbb{RIX}$, which can be estimated directly from option prices. This index builds on the jump and tail risk index $\mathbb{JTIX}$ suggested by Kapadia and Du (2012) and measures—intuitively speaking—the difference between the quadratic variation of stock price returns with and without event risk. However, to accurately calculate the $\mathbb{RIX}$ a continuum of option prices is required.

The focus of this paper is on the estimation of the rare disaster concern index $\mathbb{RIX}$ when a continuum of option prices is not available. In practice, this problem is particularly relevant for options on single stocks but also—to a lesser extent—for index options. Single stock options are less liquidly traded than index options. For this reason, the range of available strike prices of options on single stocks is smaller than for index options. This is critical for the estimated $\mathbb{RIX}$ since the index depends significantly on the prices of deep out-of-the-money (OTM) put options. Therefore, economically reasonable extrapolation techniques are required to estimate option prices beyond the available strike range. Another consequence of lower trading volumes is more market-microstructure noise that might lead to further distortions of estimated $\mathbb{RIX}$. Robust inter- and extrapolation techniques are required to deal with such noise in prices.

This study provides three main contributions. First, we develop a new approach to the construction of a continuous implied volatility smile from noisy option prices based on the risk-neutral return distribution (RND).[3] This approach is needed to extrapolate far OTM put option prices required for the accurate estimation of the $\mathbb{RIX}$ from the range of available option prices. Inspired by Birru and Figlewski (2012), we model the tails of the RND using the Generalized Extreme Value (GEV) distribution to extrapolate the implied volatilities of OTM options. This new optimization approach makes sure that the transition between the extrapolated and observable part of the volatility smile is always continuous. The extrapolation technique requires smoothing of observable implied volatilities. We use a cubic spline with additional convexity constraints in the spirit of Fengler (2009). This ensures that the underlying RND is well-behaved in the presence of microstructure noise.

Second, we benchmark our RND-tail-modeling approach to standard extrapolation techniques from the literature. These are endpoint volatility and linear extrapolation. Endpoint volatility assumes that the smile is flat beyond the observable range of option prices. Linear extrapolation extends the range assuming a linear relation between moneyness and implied volatilities. Both approaches are popular choices in the academic literature as well as in practice. While endpoint volatility produces relatively high but stable $\mathbb{RIX}$ estimation errors, linear regression proves to be more accurate but highly unstable in the presence of microstructure noise. It turns out that the RND-tail extrapolation approach combines the favorable properties of both endpoint volatility and linear extrapolation. We show that it (1) substantially mitigates the bias induced by endpoint volatility and (2) is considerably more robust to microstructure noise than linear extrapolation. This proves particularly advantageous to the modeling of deep in- and out-of-the-money option volatilities. We find that RND-tail modeling is the superior approach to the estimation of the $\mathbb{RIX}$ and similar metrics when event risk is high—the type of risk these metrics are supposed to measure.

Third, we empirically apply the RND-based smile construction approach to options written on the set of *FAANG* stocks.[4] We mimic the two scenarios in the numerical analysis by considering a normal and a volatile trading day as indicated by the volatility index (VIX). For three narrowed moneyness ranges, we construct volatility smiles using the RND-based approach, endpoint volatility, and linear regression. This allows us to compute the root mean square error (RMSE) of extrapolated implied volatilities with respect to contracts outside these ranges. We find that RND-tail extrapolation matches the data considerably better than standard techniques. On the volatile trading day, the improved accuracy of the RND-based approach translates to $\mathbb{RIX}$ estimates that exceed their counterparts using endpoint volatility (linear regression) by 73.97% (18.29%) on average. Standard techniques tend to underestimate rare disaster concerns when jump and tail risks are prevalent.

This study is related to the following strands of literature: First, Carr and Madan (1998), Demeterfi et al. (1999), and Britten-Jones and Neuberger (2000) as well as Bakshi et al. (2003) deal with model-free option-implied risk-neutral moments that can be computed from a continuous range of strike prices. In particular, Gao et al. (2018) propose the rare disaster concern index ($\mathbb{RIX}$) that builds on the model-free measure of jump and tail risk of

[2]For a detailed discussion on event risk and option prices, see, for example, Backus et al. (2011) and Seo and Wachter (2019).
[3]If there is no ambiguity, the abbreviation RND may either refer to the risk-neutral probability density function (PDF) or to the RND in general.
[4]*FAANG* stands for the stocks of Facebook (Meta), Amazon, Apple, Netflix, and Google (Alphabet).

Kapadia and Du (2012). Gao et al. (2019) extend this index to a global scale. Second, Ammann and Feser (2019), Aschakulporn and Zhang (2022a), Aschakulporn and Zhang (2022b), Bliss and Panigirtzoglou (2002), Dennis and Mayhew (2009), and Jiang and Tian (2005) study implementation errors in risk-neutral moments. These emerge from approximations that are required due to the lack of a continuous strike range in practice. Different approaches to interpolation, smoothing, and extrapolation are proposed, for example, by Ait-Sahalia and Lo (1998), Carr and Wu (2009), Fengler (2009), or Jiang and Tian (2007). More recently, Aschakulporn and Zhang (2022b) analyze numerical errors in Bakshi et al. (2003) risk-neutral moments based on the parametric Duffie et al. (2000) model calibrated to S&P 500 data. Moreover, Aschakulporn and Zhang (2022a) also propose an analytical $\mathbb{RIX}$ formula for the whole domain of option prices using the Gram–Charlier density. Muck (2022) considers arbitrage-free smile construction for FX options based on the Carr and Wu (2009) near-term volatility dynamics. Third, a large body of literature focuses on the estimation of the full RND from option prices. Shimko (1993) combines the interpolation of implied volatilities by a quadratic polynomial with log-normal tail extrapolation. Bahra (1997) applies a cubic spline for smile interpolation and a mixture of two log-normal distributions to enhance RND-tail modeling. More recently, Birru and Figlewski (2012) use the GEV distribution analyzed by Bali (2003) to model the tails of the RND.

This study is organized as follows. Section 2 outlines how jump and tail risk can be extracted using option-based model-free measures and discusses estimation errors induced by standard smile extrapolation techniques. Section 3 develops an arbitrage-free implied volatility smile construction approach involving extrapolation by RND-tail modeling and interpolation and smoothing of observable implied volatilities. Section 4 introduces a benchmark model and scenarios, conducts a numerical analysis of estimation errors for different extrapolation and smoothing techniques, and performs a simulation study to shed light on the importance of microstructure noise. Section 5 empirically applies the RND-based smile construction approach to a set of individual stocks and compares its performance to standard techniques for a normal and a volatile trading day. Section 6 concludes.

2 | INFORMATION ON JUMP AND TAIL RISK IN OPTION PRICES

In this section, we outline how jump and tail risk can be extracted from option prices. Section 2.1 deals with the model-free approach to recover risk-neutral moments from option prices, summarizes the jump and tail risk measure $\mathbb{JTIX}$ of Kapadia and Du (2012) and presents corresponding option-based estimators as well as the rare disaster concern index $\mathbb{RIX}$ of Gao et al. (2018, 2019). Section 2.2 discusses the impact numerical implementation techniques may have on the estimation of the $\mathbb{RIX}$ and other option-based risk measures.

2.1 | Extracting information from option prices

Event risk of stock returns can be extracted from option prices. In particular, it is reflected in the implied volatility skew (Backus et al., 2011; Seo & Wachter, 2019). Statistically, Bakshi et al. (2003) (BKM) identify negative skewness and fat tails of the RND as drivers of the typically asymmetric shape of the implied volatility smile.[5] Thus, implied volatilities of far OTM call and put options contain information on tail risk in the RND and on event risk in stock indices and individual equities.

Kapadia and Du (2012) propose a measure of jump and tail risk that does not rely on specific parametric assumptions. It builds on model-free estimators from the literature that recover moments of the RND from OTM option prices directly. Intuitively speaking, it is the difference between the quadratic variation of stock price returns with and without event risk. The key insight is that—when there is no jump risk—both measures of quadratic variation are identical for short maturities. To begin with, Bakshi et al. (2003) propose to estimate (higher-order) risk-neutral moments from option prices. These include skewness, kurtosis, and the holding-period return variance

[5]Bakshi et al. (2003) point out that the RNDs of individual stocks and stock indices differ with respect to higher moments implied by the corresponding option contracts.

$$\text{var}_0^{\mathbb{Q}}\left[\ln\left(\frac{S_T}{S_0}\right)\right] = E_0^{\mathbb{Q}}\left[\ln\left(\frac{S_T}{S_0}\right)^2\right] - E_0^{\mathbb{Q}}\left[\ln\left(\frac{S_T}{S_0}\right)\right]^2, \tag{1}$$

where S_t denotes the time-t stock price that follows a potentially noncontinuous càdlàg process, $E_t^{\mathbb{Q}}[\cdot]$ the time-t conditional expectation under the risk-neutral measure $\mathbb{Q}$, and T the time horizon of interest.[6] Kapadia and Du (2012) point out that the risk-neutral holding-period variance captures jump risk. For the entire class of Lévy processes, this variance is an unbiased estimator of return quadratic variation:

$$E_0^{\mathbb{Q}}[\ln S, \ln S]_T = \text{var}_0^{\mathbb{Q}}\left[\ln\left(\frac{S_T}{S_0}\right)\right]. \tag{2}$$

If volatility is stochastic, there is an approximation error that is negligible for short maturities, though.

Carr and Madan (1998), Demeterfi et al. (1999), and Britten-Jones and Neuberger (2000) propose the integrated variance of a continuous process as a measure of quadratic variation. It captures stochastic volatility but is only exact in the absence of discontinuities. However, for the noncontinuous process S_t the corresponding estimator of quadratic variation is biased. It is given by

$$E_0^{\mathbb{Q}}[\ln S, \ln S]_T^c = 2E_0^{\mathbb{Q}}\left[\int_0^T \frac{1}{S_{t^-}} dS_t - \ln\left(\frac{S_T}{S_0}\right)\right], \tag{3}$$

where S_{t^-} is the stock price before any jump at time t. Even though the VIX is based on $E_0^{\mathbb{Q}}[\ln S, \ln S]_T^c$, it is frequently used as a general measure of quadratic variation.[7] Kapadia and Du (2012) propose to use the difference between the holding-period return variance (1) and the VIX-type estimator of quadratic variation (3) as their jump and tail risk index

$$\begin{aligned}\mathbb{JTIX} &= \text{var}_0^{\mathbb{Q}}\left[\ln\left(\frac{S_T}{S_0}\right)\right] - E_0^{\mathbb{Q}}[\ln S, \ln S]_T^c \\ &= E_0^{\mathbb{Q}}\left[\ln\left(\frac{S_T}{S_0}\right)^2\right] - E_0^{\mathbb{Q}}\left[\ln\left(\frac{S_T}{S_0}\right)\right]^2 - 2E_0^{\mathbb{Q}}\left[\int_0^T \frac{1}{S_{t^-}} dS_t - \ln\left(\frac{S_T}{S_0}\right)\right].\end{aligned} \tag{4}$$

Equation (4) can be computed using a replication portfolio of options. Gao et al. (2018, 2019) adopt the approach of Kapadia and Du (2012) and obtain the annualized risk-neutral holding-period return variance using

$$\mathbb{V} \equiv 2\frac{e^{rT}}{T}\left[\int_{K>S_0} \frac{1-\ln(K/S_0)}{K^2} C(S_0; K, T)\, dK + \int_{K<S_0} \frac{1-\ln(K/S_0)}{K^2} P(S_0; K, T)\, dK\right], \tag{5}$$

where r is the risk-free interest rate with continuous compounding and $C(S_0; K, T)$ and $P(S_0; K, T)$ are the prices of European-style call and put options with strike price K and maturity date T.[8] In contrast to the option-based estimator of Kapadia and Du (2012), $\mathbb{V}$ is not centered with respect to the square of the risk-neutral expected log return. Gao et al. (2018) further replicate the VIX-type integrated variance estimator $E_0^{\mathbb{Q}}[\ln S, \ln S]_T^c$ as

$$\mathbb{IV} \equiv 2\frac{e^{rT}}{T}\left[\int_{K>S_0} \frac{1}{K^2} C(S_0; K, T)\, dK + \int_{K<S_0} \frac{1}{K^2} P(S_0; K, T)\, dK\right]. \tag{6}$$

[6]For simplicity, we consider the case $t = 0$ which can be generalized to arbitrary times t. For general t it is understood that T is some future point in time and that formulas that depend on the time span $T - t$ must be adjusted accordingly.

[7]See, for example, Bollerslev et al. (2011), Carr and Wu (2009), or Jiang and Tian (2005).

[8]As we consider the case when $t = 0$, T denotes both the time when and until the option expires. For general t, time to expiration is usually different from the option expiry T.

In fact, the square-root of $\mathbb{IV}$ (multiplied by 100) is equal to the CBOE VIX that is calculated from options on the S&P 500 index.

We follow Gao et al. (2018) and focus on negative price deviations. They obtain downside versions of $\mathbb{V}$ and $\mathbb{IV}$ by constructing replication portfolios from European-style OTM put options only:

$$\begin{aligned}\mathbb{V}^- &\equiv 2\frac{e^{rT}}{T}\int_{K<S_0}\frac{1-\ln(K/S_0)}{K^2}P(S_0;\,K,\,T)\,dK\\ \mathbb{IV}^- &\equiv 2\frac{e^{rT}}{T}\int_{K<S_0}\frac{1}{K^2}P(S_0;\,K,\,T)\,dK.\end{aligned} \tag{7}$$

In analogy to Equation (4), the difference between $\mathbb{V}^-$ and $\mathbb{IV}^-$ captures the risk of downside rare events. Gao et al. (2018) label this difference the rare disaster concern index ($\mathbb{RIX}$)

$$\mathbb{RIX} = \mathbb{V}^- - \mathbb{IV}^- = 2\frac{e^{rT}}{T}\int_{K<S_0}\frac{\ln(S_0/K)}{K^2}P(S_0;\,K,\,T)\,dK. \tag{8}$$

They state that it serves as a forward-looking measure for variations in disaster concerns and can be seen as the current price of insurance against extreme future downside movements.

2.2 | Standard implementation techniques and $\mathbb{RIX}$ estimation errors

The $\mathbb{RIX}$ as well as $\mathbb{V}$, $\mathbb{IV}$, $\mathbb{V}^-$, and $\mathbb{IV}^-$ require that option prices are available for a continuum of strike prices. Since this prerequisite is not fulfilled in the market, the implementation of the replication portfolios requires the combined application of different numerical approximation techniques. A growing literature analyzes the impact of implementation errors on option-based risk measures.[9] They mainly consider truncation errors caused by a limited moneyness range, curve fitting errors from interpolation or smoothing discretely spaced strike prices, and measurement errors induced by microstructure noise.[10]

The majority of these studies focus on index option contracts in the usual moneyness range around the spot price but rely on standard techniques for smile extrapolation. These include the endpoint volatility (flat extrapolation, EndPoint) and linear regression (linear extrapolation, LinReg) approaches. First, endpoint volatility extends the smile by assuming that implied volatilities remain constant at the outermost observable level (Gao et al., 2018, 2019; Jiang & Tian, 2005). The steeper the "true" smile, the greater is the bias that is induced by this approximation. Second, linear extrapolation estimates the slope of the smile at its outer strikes and uses the estimate to linearly extend the smile beyond these points (Jiang & Tian, 2007). Approximation errors can result from the curvature of the smile or from noisy estimates of the slope coefficients. Aschakulporn and Zhang (2022b) and Ammann and Feser (2019) consider both approaches and point out that linear extrapolation reduces the bias induced by endpoint volatility but may generate negative implied volatilities and is highly sensitive to microstructure noise. In a similar vein, Gao et al. (2018, 2019) apply endpoint volatility to obtain their estimates of the $\mathbb{RIX}$.

Higher-order moments and, in particular, tail and jump risk measures are prone to extrapolation errors. These can translate to inaccuracies in metrics, like, the $\mathbb{RIX}$. The problem is typically aggravated for sparsely observed individual options and can become a critical issue when model-free metrics serve as inputs.[11] The aforementioned standard techniques are often considered as reasonable for smile construction due to their simplicity. However, a major caveat is

[9]Jiang and Tian (2005) conduct their analysis for the VIX-type estimator of integrated variance. Dennis and Mayhew (2009) focus on the Bakshi et al. (2003) risk-neutral moment estimators and find that implementation errors may induce significant biases even if option prices are observed without any noise. Ammann and Feser (2019) provide a comprehensive comparison of errors in option-implied higher moments resulting from different implementation techniques.

[10]Some studies also address discretization errors resulting from numerical integration (see, e.g., Jiang & Tian, 2005). We neglect this type of error since we presume that interpolation yields a grid of option prices that is sufficiently dense to ensure highly accurate approximations.

[11]For example, the normal inverse Gaussian (NIG) distributions proposed by Eriksson et al. (2009) to approximate unknown RND build on model-free Bakshi et al. (2003) higher-order moments. To extrapolate the volatility smile, Eriksson et al. (2009) rely on the simple endpoint volatility approach, though. This assumes that implied volatility remains constant beyond the observable range.

that the resulting prices may admit arbitrage. In particular, these procedures lead to inconsistencies between the tails and the central part of the risk-neutral density.

3 | RND-CONSISTENT SMILE CONSTRUCTION

In this section, we introduce an RND-consistent smile construction approach that aims at improving estimates of tail risk measures like the $\mathbb{RIX}$ for illiquid and sparsely sampled option contracts. This ensures that option prices are free from arbitrage. Section 3.1 briefly summarizes the one-to-one relation between option-implied volatilities and the underlying RND, Section 3.2 details the approach to smile extrapolation by RND-tail modeling, and Section 3.3 discusses interpolation and smoothing procedures required to make the RND-based approach applicable for a limited set of observable option prices that are affected by microstructure noise.

3.1 | Option-implied RND

There is a one-to-one relation between the implied volatility smile and the underlying RND. In particular, the wings of the smile drive the tails of the RND. Under the assumption of no-arbitrage, the RND is defined as the probability distribution under the risk-neutral measure $\mathbb{Q}$.[12] For example, the price of a European-style put option with strike K and maturity T can be expressed in terms of the RND:

$$P(S_0; K, T) = e^{-rT}\mathbb{E}_0^{\mathbb{Q}}[(K - S_T)^+] = e^{-rT}\int_0^K (K - S_T) f(S_T)\, dS_T, \tag{9}$$

where $f(S_T)$ denotes the risk-neutral PDF of the stock price S_t at expiration T. As shown by Breeden and Litzenberger (1978), the cumulative distribution function (CDF) $F(S_T)$ and the density $f(S_T)$ evaluated at some strike K follow from the first- and second-order derivatives of the option price with respect to this strike:

$$\begin{aligned} F(K) &= e^{rT}\frac{\partial P(S_0; K, T)}{\partial K}, \\ f(K) &= e^{rT}\frac{\partial^2 P(S_0; K, T)}{\partial K^2}. \end{aligned} \tag{10}$$

The CDF and PDF in Equation (10) can be approximated by finite differences. Consider N evenly spaced option prices with strike prices $K_1, K_2, ..., K_N$ in ascending order and let $\Delta K = K_{n+1} - K_n$. For some strike K_n we then get

$$\begin{aligned} \hat{F}(K_n) &= e^{rT}\frac{P(S_0; K_{n+1}, T) - P(S_0; K_{n-1}, T)}{2\Delta K}, \\ \hat{f}(K_n) &= e^{rT}\frac{P(S_0; K_{n+1}, T) - 2P(S_0; K_n, T) + P(S_0; K_{n-1}, T)}{(\Delta K)^2}, \end{aligned} \tag{11}$$

where $\hat{F}(K_n)$ and $\hat{f}(K_n)$ are the approximated risk-neutral CDF and PDF, respectively.

3.2 | RND-tail modeling

In the following, we present the approach to smile extrapolation by RND-tail modeling. We assume that option prices are available for a dense grid of evenly spaced strike prices $K_1, K_2, ..., K_N$ and that the moneyness range is

[12] $\mathbb{Q}$ is an equivalent martingale measure with respect to the physical measure $\mathbb{P}$. The RND can be seen as the objective estimate of the underlying probability distribution adjusted for investor risk-preferences.

limited. Further, the underlying RND implied by available option prices is well-behaved. We focus on extrapolation first. The handling of errors induced by strike spacing and microstructure noise is treated in the subsequent Section 3.3.

Observable option prices do not imply specific distributional assumptions for the underlying RND. A tail-modeling approach must thus be sufficiently flexible to capture different stylized facts of the data. We follow Birru and Figlewski (2012) and apply the GEV distribution. The GEV is highly flexible and nests the Gumbel, the Fréchet, and the reversed Weibull distribution as special cases. It is characterized by three parameters that control location (μ), scale (σ), and shape (ξ). The parameter ξ determines the specific type of GEV and thus its tail behavior. The corresponding PDF $f_{GEV}(x)$ and CDF $F_{GEV}(x)$ are given in Appendix A.1.

Our goal is to extrapolate implied volatilities such that the corresponding OTM option prices do not admit arbitrage. Therefore, we require that the RND satisfies the probability axioms of Kolmogorov as well as the martingale property (Brunner & Hafner, 2003). Specifically, the risk-neutral density $f(S_T)$ must be nonnegative

$$f(S_T) \geq 0 \quad \forall\, S_T \geq 0 \tag{12}$$

and integrate to one

$$\int_0^\infty f(S_T)\, dS_T = 1. \tag{13}$$

Further, the martingale property requires that the RND prices options correctly when $K = 0$. As outlined by Brunner and Hafner (2003), this implies that the risk-neutral expectation of S_T equals the current price of a forward contract with maturity in T,

$$\mathbb{E}_0^{\mathbb{Q}}[S_T] = S_0 e^{rT}. \tag{14}$$

The GEV can be used to model the *right* tail of the RND corresponding to OTM call options directly (Birru & Figlewski, 2012). We connect the GEV tail to the RND implied by available option prices under two requirements. First, consistent with Birru and Figlewski (2012), PDF and CDF values from the GEV and available option prices must coincide at the connection strike price K_{N-1} to obtain well-behaved RND tails. Second, to satisfy the martingale property, the call option price at the outermost available strike price K_N computed from the GEV tail $C_{GEV}(S_0; K_N, T)$ must be equal to the outermost available call option price $C(S_0; K_N, T)$. The second requirement is crucial to ensure that at the connecting strike price K_N GEV-implied and observable implied volatilities are identical such that the extrapolated volatility smile is actually continuous. This second requirement is a modification of Birru and Figlewski (2012) who impose further restrictions on the PDF. Their approach does not guarantee a continuous volatility smile, as outlined in Section 4.2, though.

The optimization problem for the right tail then reads

$$\begin{aligned} \underset{\mu,\sigma,\xi}{\arg\min} \quad & \left(C_{GEV}(S_0; K_N, T) - C(S_0; K_N, T)\right)^2 \\ \text{subject to} \quad & f_{GEV}(K_{N-1}) = \hat{f}(K_{N-1}), \\ & F_{GEV}(K_{N-1}) = \hat{F}(K_{N-1}), \end{aligned} \tag{15}$$

where

$$C_{GEV}(S_0; K_N, T) = e^{-rT} \int_{K_N}^\infty (S_T - K_N) f_{GEV}(S_T)\, dS_T.$$

To model the *left* tail of the RND that corresponds to OTM put options the GEV must be defined on $-S_T$ and $-\mu$. Analogously, (1) PDF and CDF values from the GEV and available options must coincide at the connecting strike price K_2 and (2) the price of the put option with strike K_1 implied by the GEV tail $P_{GEV}(S_0; K_1, T)$ must equal the outermost available put price $P(S_0; K_1, T)$. The left tail optimization problem reads accordingly

$$\begin{aligned} \underset{-\mu,\sigma,\xi}{\arg\min} \quad & (P_{GEV}(S_0; K_1, T) - P(S_0; K_1, T))^2 \\ \text{subject to} \quad & f_{GEV}(-K_2) = \hat{f}(K_2), \\ & 1 - F_{GEV}(-K_2) = \hat{F}(K_2), \end{aligned} \tag{16}$$

where

$$P_{GEV}(S_0; K_1, T) = e^{-rT} \int_0^{K_1} (K_1 - S_T) f_{GEV}(-S_T)\, dS_T.$$

3.3 | Interpolation and smoothing observed implied volatilities

The extrapolation outlined above cannot be applied to market data directly. In practice, option prices are affected by microstructure noise and trading is limited to a discrete grid of unequally spaced and sparsely sampled strikes. For such data, the finite-differences approximation of the risk-neutral PDF and CDF values at the connecting strikes K_2 and K_{N-1} is either infeasible or significantly affected by noise. Interpolation and smoothing of the observed implied volatilities are thus necessary.

One of the most popular techniques for solving this task is a natural cubic smoothing spline. While the smoothing works well for financial applications in the implied volatility domain, the resulting RND can exhibit large spikes and is highly sensitive towards the choice of the smoothing parameter (Figlewski, 2018). To ensure that suitable estimates of option prices and risk-neutral PDF and CDF values are available as inputs to our extrapolation approach, we enforce an additional convexity constraint along the lines of Fengler (2009). This is achieved by imposing bounds on the second-order derivatives of the spline which, as pointed out by Dole (1999), act as strong constraints on the roughness of the spline. Thus, the overall sensitivity towards the explicit smoothing parameter is reduced. While Fengler (2009) developed this approach for option prices, we apply it to implied volatilities directly to obtain a smooth smile from noisy observations. This is equivalent to assuming that the observable (central) part of the volatility smile is always convex. We consider this restriction acceptable as it is mostly supported by the data and the main focus is on improving the extrapolation of implied volatilities. Details on the cubic smoothing spline with additional convexity constraints can be found in Appendix A.2.

4 | NUMERICAL ANALYSIS

In this section we numerically compare errors in estimates of risk-neutral moment-based measures that are obtained using the RND-tail-modeling extrapolation approach to their counterparts resulting from standard techniques. We focus on estimates of the rare disaster concern index $\mathbb{RIX}$, the quadratic variation $\mathbb{V}$, and the VIX-type integrated variance $\mathbb{IV}$ in our base case and crisis scenarios. Section 4.1 introduces the benchmark model and scenarios. Section 4.2 addresses the RND-tail-modeling approach of Birru and Figlewski (2012) and unveils its shortcomings within the scope of smile extrapolation. Section 4.3 deals with errors from approximating the integrals in Equations (5), (6), and (8) based on limited ranges of strike prices that are extended by extrapolation. Section 4.4 considers the combined error from truncation and strike spacing. Section 4.5 conducts a simulation study to analyze how random noise in implied volatilities affects the estimation errors.

4.1 | Benchmark model and scenarios

Similar to Aschakulporn and Zhang (2022b), we assume that option prices are generated by the Duffie et al. (2000) affine jump-diffusion model with stochastic volatility and contemporaneous jumps (SVCJ). Thus, this model is sufficiently rich to produce various shapes of potentially asymmetric volatility smiles.[13] We calibrate the

[13]Similar models are used in related studies in the literature. For example, Ammann and Feser (2019) use the Bates (1996) model in their comprehensive analysis of different implementation methods.

SVCJ model on Apple's stock options on two different trading days to create a base case and a crisis scenario.[14] Figure 1 shows the two volatility smiles (left panel) alongside with the underlying risk-neutral densities (right panel) in the two scenarios. As indicated by the wings of the smiles and the density tails, the two settings differ with respect to higher-order risk-neutral moments. Estimates of the Bakshi et al. (2003) risk-neutral moments are $\text{Var}^{\mathbb{Q}}/T = 0.1116$ (annualized), $\text{Skew}^{\mathbb{Q}} = -1.1993$, and $\text{Kurt}^{\mathbb{Q}} = 6.5872$ in the base case and $\text{Var}^{\mathbb{Q}}/T = 0.1157$, $\text{Skew}^{\mathbb{Q}} = -2.4563$ and $\text{Kurt}^{\mathbb{Q}} = 19.7374$ in the crisis scenario.[15] Thus, the crisis scenario implies that the RND has more variance, is more left-skewed, and is more leptokurtic than the one considered in the base case. The implied risk-neutral skewness matches observations of the CBOE SKEW index during normal and crisis times. Moreover, the skewness is in line with Aschakulporn and Zhang (2022b) in both scenarios. Details on the model and the two scenarios are given in Appendix A.3.

To obtain estimation errors with respect to the benchmark scenarios, we follow Ammann and Feser (2019) and compute percentage errors for different risk-neutral moment-based measures:

$$100 \times \frac{|\widehat{\mathcal{Y}} - \mathcal{Y}_{\text{dense}}|}{\mathcal{Y}_{\text{dense}}}, \quad \mathcal{Y} = \mathbb{V}, \mathbb{IV}, \mathbb{RIX}, \tag{17}$$

where $\widehat{\mathcal{Y}}$ is the candidate estimate and $\mathcal{Y}_{\text{dense}}$ is its benchmark obtained from the full range of SVCJ OTM option prices. In our numerical implementation, we use a grid size of $\Delta K/S_0 = 0.1\%$ and a spot moneyness range of $[0.01, 1.99]$. According to Aschakulporn and Zhang (2022a), skewness approximation errors are smaller than 10^{-3} for the applied grid size provided a moneyness range of at least 3/4–4/3 of the forward price. Skewness is the main driver of the $\mathbb{RIX}$. As defined in Equations (5), (6), and (8), $\mathbb{V}$ and $\mathbb{IV}$ employ OTM put and call options whereas $\mathbb{RIX}$ uses OTM puts only. The percentage error depends on the size of $\mathcal{Y}_{\text{dense}}$. Table 1 shows the benchmark estimates. In the crisis scenario, $\mathbb{RIX}_{\text{dense}}$ is almost twice as large as in the base case which must be considered when comparing the percentage metric across different scenarios.

4.2 | Birru and Figlewski (2012) tail-modeling approach

Before addressing our numerical study, we compare the modified smile construction approach outlined in Section 3.2 to the one of Birru and Figlewski (2012). The most important difference is that Birru and Figlewski (2012) model the right (left) tail of the RND by parameterizing the GEV according to the CDF at strike price K_{N-1} (K_2). For the PDF, they choose the same options and another one with K_n, $2 < n < N-1$. In addition to the degrees of freedom in the selection of K_n, their approach does not guarantee that the outermost option prices at strikes K_1 and K_N can be recovered by the modeled tails. As a consequence, implied volatilities do not match at the connecting strikes K_1 and K_N. Hence, the smile is not continuous and RND tails violate no-arbitrage constraints. This can affect $\mathbb{RIX}$ estimates significantly. For the case considered in Appendix A.4, their $\mathbb{RIX}$ estimate exhibits a percentage error of 32.84%. This compares to a percentage error of 7.14% when the modified approach is applied. This suggests that the martingale property of the modified RND-tail-modeling approach is important yielding more accurate estimates of the $\mathbb{RIX}$.

[14]We calibrate the SVCJ model on individual stock options since corresponding volatility smiles exhibit higher degrees of curvature compared with volatility smirks of index options. For the identified trading days see Section 5.

[15]We obtain estimates of BKM risk-neutral moments from a fine grid ($\Delta K/S_0 = 0.1\%$) of SVCJ OTM option prices across the full moneyness range ($K_{\text{put}}/S_0 \in [0.01, 1]$, $K_{\text{call}}/S_0 \in [1, 1.99]$). Model-generated risk-neutral moments are computed using high-accuracy trapezoidal integration. The BKM moment estimators are defined by

$$\text{Var}^{\mathbb{Q}} = e^{rT}\mathcal{V}_{0,T} - \mathcal{M}_{0,T}^2, \quad \text{Skew}^{\mathbb{Q}} = \left(e^{rT}\mathcal{W}_{0,T} - 3\mathcal{M}_{0,T}e^{rT}\mathcal{V}_{0,T} + 2\mathcal{M}_{0,T}^3\right)\left(e^{rT}\mathcal{V}_{0,T} - \mathcal{M}_{0,T}^2\right)^{-3/2},$$
$$\text{Kurt}^{\mathbb{Q}} = \left(e^{rT}\mathcal{X}_{0,T} - 4\mathcal{M}_{0,T}e^{rT}\mathcal{W}_{0,T} + 6e^{rT}\mathcal{M}_{0,T}^2\mathcal{V}_{0,T} - 3\mathcal{M}_{0,T}^4\right)\left(e^{rT}\mathcal{V}_{0,T} - \mathcal{M}_{0,T}^2\right)^{-2},$$

where $\mathcal{M}_{0,T} = e^{rT} - 1 - e^{rT}/2\mathcal{V}_{0,T} - e^{rT}/6\mathcal{W}_{0,T} - e^{rT}/24\mathcal{X}_{0,T}$ and $\mathcal{V}_{0,T}, \mathcal{W}_{0,T}, \mathcal{X}_{0,T}$ are the payoffs of volatility, cubic, and quartic contracts as specified in Bakshi et al. (2003).

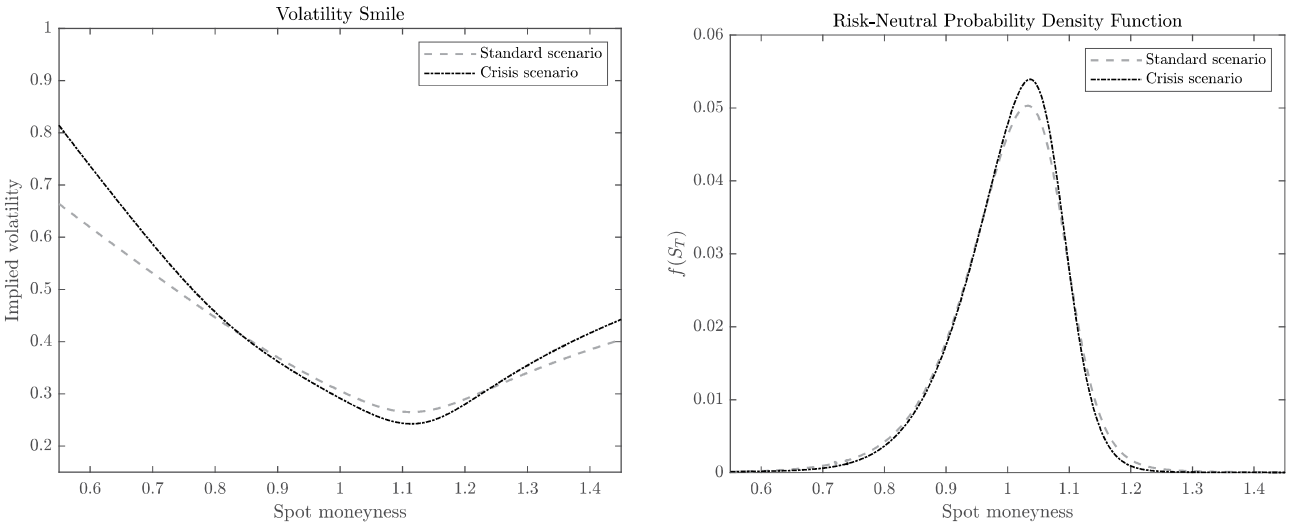

FIGURE 1 Base case and crisis benchmark scenario. The figure plots Black and Scholes (1973) volatility smiles (left panel) and underlying risk-neutral densities (right panel) implied by the SVCJ model detailed in Appendix A.3. The risk-neutral density is approximated using finite differences with a fine grid of $\Delta K/S_0 = 0.1\%$. The base case scenario emerges for $\kappa = 1.1521$, $\theta = 0.3437$, $\sigma = 0.6772$, $\rho = -0.5882$, $V_t = 0.0845$, $\lambda = 3.2642$, $\mu_X = -0.0318$, $\sigma_X = 0.0273$, $\mu_y = 0.2245$, and $\rho_J = -0.0921$. The crisis scenario differs in that $\kappa = 1.4333$, $\theta = 0.3779$, $\sigma = 0.9892$, $\rho = -0.6993$, $V_t = 0.0669$, $\lambda = 0.1876$, $\mu_X = 0.0473$, $\sigma_X = 0.2295$, $\mu_y = 0.3962$, and $\rho_J = -0.6677$. Dense-grid estimates of the risk-neutral BKM annualized variance, skewness, and kurtosis are $\text{Var}^{\mathbb{Q}}/T = 0.1116$, $\text{Skew}^{\mathbb{Q}} = -1.1993$, and $\text{Kurt}^{\mathbb{Q}} = 6.5872$ in the base case and $\text{Var}^{\mathbb{Q}}/T = 0.1157$, $\text{Skew}^{\mathbb{Q}} = -2.4563$, and $\text{Kurt}^{\mathbb{Q}} = 19.7374$ in the crisis scenario. BKM, Bakshi, Kapadia, and Madan; SVCJ, stochastic volatility and contemporaneous jump.

TABLE 1 Benchmark scenarios—Model-free measures.

	Gao et al. (2018)		
	$\mathbb{V}_{\text{dense}}$	$\mathbb{IV}_{\text{dense}}$	$\mathbb{RIX}_{\text{dense}}$
Base case	0.1117	0.1076	0.0057
Crisis	0.1158	0.1078	0.0095

Note: The table shows dense-grid ($\Delta K/S_0 = 0.1\%$) benchmark estimates of the Gao et al. (2018) model-free measures $\mathbb{V}$, $\mathbb{IV}$, and $\mathbb{RIX}$ for the base case and the crisis scenarios. All estimates are computed from the full range of SVCJ OTM option prices $K_{\text{put}}/S_0 \in [0.01, 1]$, $K_{\text{call}}/S_0 \in [1, 1.99]$ ($\mathbb{RIX}$ from OTM put options only) using trapezoidal integration.

Abbreviations: OTM, out-of-the-money; SVCJ, stochastic volatility and contemporaneous jump.

4.3 | Truncation

Table 2 shows estimation errors when available option prices are limited to moneyness ranges of ±25%, ±20%, and ±15% around the spot and extended by flat, linear, and RND-tail extrapolation.[16] In the available range, benchmark option prices are sampled at a fine grid of $\Delta K/S_0 = 0.1\%$ corresponding to 1981 equally spaced strikes for $\mathbb{V}$ and $\mathbb{IV}$ and 991 for the $\mathbb{RIX}$. Keeping the grid size, the truncated ranges reduce the number of available strikes to 501 for ±25% (251 for $\mathbb{RIX}$), 401 for ±20% (201 for $\mathbb{RIX}$), and 301 for ±20% (151 for $\mathbb{RIX}$). Extrapolation is then used to recover the range of 1981 (991) strikes. All estimates result from trapezoidal integration without interpolation or smoothing. Intuitively, errors increase when the observable range of option prices becomes narrower. Without the usual strike spacing or microstructure noise, extrapolation by RND-tail modeling is superior to the standard methods in both scenarios. This finding can be attributed to several reasons.

[16]Ammann and Feser (2019) show $\mathbb{RIX}$ estimation errors for moneyness ranges ("domain half-width") of −10%, −50%, and −80% and report that $\mathbb{RIX}$ estimates become stable at −50%. In contrast, we focus on ranges between −25% and −15% as we consider these more realistic in light of available data.

TABLE 2 Estimation errors model-free measures—Truncation.

	$\mathbb{V}$			$\mathbb{IV}$			$\mathbb{RIX}$		
Observable range	**±25%**	**±20%**	**±15%**	**±25%**	**±20%**	**±15%**	**−25%**	**−20%**	**−15%**
Panel A: Base case scenario									
EndPoint	1.6633	3.2640	5.8731	1.2830	2.6147	4.8715	8.7915	15.5398	24.7732
LinReg	0.0643	0.2564	0.8710	0.0409	0.1980	0.7628	0.4322	1.3784	3.6738
RND	0.0682	0.2000	0.1929	0.0506	0.1552	0.1109	0.4046	1.1134	1.4192
Panel B: Crisis scenario									
EndPoint	10.0051	12.7714	16.1127	7.1999	9.5510	12.5204	41.4249	48.9764	56.5466
LinReg	2.8324	5.6067	9.1906	1.1288	3.2268	6.7437	15.8089	26.8983	37.1497
RND	0.1001	1.3119	3.9015	0.0666	0.8544	2.8208	2.2844	7.1419	16.3818

Note: The table shows percentage errors $100 \times |\widehat{\mathcal{Y}} - \mathcal{Y}_{\text{dense}}|/\mathcal{Y}_{\text{dense}}$ for $\mathcal{Y} = \mathbb{V}, \mathbb{IV}, \mathbb{RIX}$ using endpoint volatility (EndPoint), linear regression (LinReg), and RND-tail (RND) extrapolation for the base case (Panel A) and crisis scenario (Panel B). $\mathcal{Y}_{\text{dense}}$ is the respective benchmark computed from the full range of SVCJ OTM option prices $K_{\text{put}}/S_0 \in [0.01, 1]$, $K_{\text{call}}/S_0 \in [1, 1.99]$ ($\mathbb{RIX}$ from OTM put options only), and $\widehat{\mathcal{Y}}$ is the estimate from the truncated and extrapolated volatility smile. Errors are shown for observable moneyness ranges $[K_{\text{put}}^{\min}/S_0, K_{\text{call}}^{\max}/S_0]$ of [0.75, 1.25] (±25%), [0.8, 1.2] (±20%), [0.85, 1.15] (±15%) where $\mathbb{RIX}$ uses OTM put options only. $\mathcal{Y}_{\text{dense}}$ and $\widehat{\mathcal{Y}}$ follow from trapezoidal integration across dense grids of strikes with $\Delta K/S_0 = 0.1\%$.

Abbreviations: OTM, out-of-the-money; RND, risk-neutral return distribution; SVCJ, stochastic volatility and contemporaneous jump.

First, *endpoint volatility* extends the truncated smiles using implied volatilities at the outermost strikes K_1 and K_N, only. The narrower the available range of option prices, the larger the error. Deviations from the benchmark smiles are more important in the crisis scenario than in the base case since the steepness of the former leads to implied volatilities and option prices that are too low. The tails of the underlying RND are underestimated which is more pronounced for the left tail due to negative risk-neutral skewness in the distribution. As the $\mathbb{RIX}$ is computed based on OTM put options only, the resulting asymmetric smile in the crisis scenario leads to estimation errors up to 56.55% compared with 24.77% in the base case. With respect to truncation, endpoint volatility has the highest errors when computing the $\mathbb{RIX}$. With endpoint volatility, $\widehat{\mathbb{RIX}}$ is the least accurate when there is a significant jump risk—the type of risk it is supposed to measure.

Second, *linear extrapolation* determines the slope of the smile outside the available range from the two outermost strikes on each side K_1, K_2, K_{N-1}, and K_N. The bias due to truncation is substantially reduced for all model-free measures in both scenarios. Due to the curvature of the benchmark smiles, errors increase when the moneyness range becomes narrower. As the crisis scenario exhibits a higher degree of convexity, linear extrapolation generates errors up to 37.15% compared with 3.67% in the base case. Linear extrapolation is thus superior to endpoint volatility when there is no microstructure noise and strikes are densely sampled.

Third, *RND-tail-modeling* parameterizes the GEV based on the outermost option prices at the strikes K_1 and K_N as well as on the PDF and CDF values of the RND at K_2 and K_{N-1}. In the base case, the GEV tails reproduce the less curved implied volatility smile with small percentage errors. $\mathbb{RIX}$ errors in absolute terms are slightly smaller compared with those from linear extrapolation. In the crisis scenario, the steeper smile with a more pronounced degree of curvature implies higher option prices that are reflected in the PDF and CDF of the RND. Due to its flexibility, the GEV is capable to produce different shapes of the RND. This leads to considerably lower errors and a less severe impact of the truncation range compared with standard extrapolation methods.

4.4 | Strike spacing

We extend the prior analysis to grids with a more realistic strike spacing. In addition to limiting the moneyness range, we now assume equally spaced grids with $\Delta K/S_0 = 1\%, 2\%$, and 5%. This further reduces the number of observable contracts for the computation of $\mathbb{V}$ and $\mathbb{IV}$ ($\mathbb{RIX}$) down to $\tilde{N} = 7$ ($\tilde{N} = 4$) for ±15% (−15%) and $\Delta K/S_0 = 5\%$. To approximate the estimators defined in Equations (5), (6), and (8), we first apply natural cubic spline interpolation to the observable implied volatilities. This generates a dense grid of strike prices. Due to the absence of microstructure noise,

smoothing is not required.[17] Then, extrapolation is applied along the lines of Section 4.3 and $\mathbb{V}$, $\mathbb{IV}$, and $\mathbb{RIX}$ are computed using trapezoidal integration.

Table 3 shows the results. For simplicity, we assume that changing the grid size does not affect the outermost strikes $K_1 = \tilde{K}_1$ and $K_N = \tilde{K}_{\tilde{N}}$. As the natural cubic spline passes exactly through all observable implied volatilities, the results for *endpoint volatility* are comparable to those in Table 2. For *linear regression* the impact of coarser strike grids is also limited. The slope of the linear extrapolation is derived from the two outermost available strikes on each side of the smile *after* interpolation. Errors are mainly determined by the interplay between the curvature of the benchmark smile and the width of the observable moneyness range. Further, the natural cubic spline minimizes the curvature of its piecewise polynomials which may lead to an underestimation of the curvature of the benchmark smile. As a consequence, the impact of the strike spacing is stronger in the crisis scenario than in the base case.

Errors from RND-tail modeling are more sensitive with respect to the strike spacing. In the base case, the percentage errors increase slightly but remain smaller than those from linear extrapolation for almost every moneyness range/strike spacing combination. In the crisis scenario, percentage errors are considerably lower and tend to increase with the widening strike spacing up to the level of their linear extrapolation counterparts for $\Delta K/S_0 = 5\%$. Errors from linear extrapolation are higher but remain at the same level for differently spaced strikes. The main reason for this pattern in RND-tail-modeling estimation errors is that this extrapolation technique depends on risk-neutral PDF and CDF values. While implied volatilities at $\tilde{K}_1 = K_1$ and $\tilde{K}_{\tilde{N}} = K_N$ are not distorted, PDF and CDF values are highly sensitive to the interpolation procedure at the connecting strikes K_2 and K_{N-1}. Small changes in the slope or curvature of the smile affect the finite differences approximation of the PDF and CDF values which then enter the optimization problem that determines the GEV parameters directly. Thus, RND-tail modeling yields different errors in comparison to the dense-grid benchmark estimates.

In the absence of noise, linear or RND-tail extrapolation should be preferred over endpoint volatility when computing tail risk measures, like, the $\mathbb{RIX}$. In the crisis scenario, errors from RND extrapolation are smaller than those generated by standard extrapolation methods. As metrics like the $\mathbb{RIX}$ depend on the accuracy of extrapolation to capture jump risk, RND-tail modeling yields better results when the RND features negative skewness and excess kurtosis.

4.5 | Microstructure noise

An obvious concern with respect to linear extrapolation is its high sensitivity to microstructure noise (see, e.g., Ammann & Feser, 2019). We, therefore, conduct a simulation study to shed light on the impact of noise on percentage errors when endpoint volatility, linear, and RND-tail extrapolation are applied to estimate $\mathbb{V}$, $\mathbb{IV}$, and $\mathbb{RIX}$. For each moneyness range and strike spacing we generate randomly perturbed implied volatilities $\tilde{\sigma}_{\text{noisy},i}$ according to

$$\tilde{\sigma}_{\text{noisy},i} = \tilde{\sigma}_i(1 + \theta\eta), \quad i = 1, ..., \tilde{N}, \tag{18}$$

where $\tilde{\sigma}_i$ are the Black and Scholes (1973) implied volatilities from SVCJ option prices in the base case and crisis scenario, $\eta \sim \mathcal{N}(0, 1)$ is a normally distributed random number, θ controls the amount of noise and $\tilde{\sigma}_{\text{noisy},i}$ are the resulting noisy observations. This approach differs from the existing literature which adds noise to option *prices* rather than to implied volatilities. The measurement errors generated by Equation (18) increase with the level of implied volatility. This mimics the common observation that bid–ask spreads are usually wider for far OTM contracts. Figure 2 illustrates the benchmark implied volatility smiles in the base case and the crisis scenario with 95% confidence intervals of noisy observations for $\theta = 2\%$. This implies that, for $\tilde{\sigma}_i = 30\%$, for example, the perturbed $\tilde{\sigma}_{\text{noisy},i}$ will lie within a bid–ask spread of about 2.35% or less with 95% probability ($\leq$1.18% for $\theta = 1\%$ and $\leq$3.53% for $\theta = 3\%$).[18]

Table 4 shows average estimation errors for $\mathbb{V}$, $\mathbb{IV}$, and $\mathbb{RIX}$ based on 1000 sets of perturbed implied volatilities with microstructure noise when $\theta = 2\%$. Error standard deviations are given in parentheses. Tables A3 and A4 in the appendix report the results for $\theta = 1\%$ and 3%. As before, we vary the moneyness range and the strike spacing to study how the interplay between different sources of error affects estimates obtained from endpoint volatility, linear

[17]As outlined in Appendix A.2, the natural cubic spline arises from Equation (A5) for $\lambda = 0$.
[18]For 40%, this spread amounts to $\leq$3.14 for $\theta = 2\%$ ($\leq$1.57% for $\theta = 1\%$ and $\leq$4.70% for $\theta = 3\%$) with 95% probability.

TABLE 3 Estimation errors model-free measures—Strike spacing.

	$\mathbb{V}$			$\mathbb{IV}$			$\mathbb{RIX}$		
Observable range	**±25%**	**±20%**	**±15%**	**±25%**	**±20%**	**±15%**	**−25%**	**−20%**	**−15%**
Panel A: Base case scenario									
$\Delta K/S_0 = 1\%$	$\tilde{N} = 51$	$\tilde{N} = 41$	$\tilde{N} = 31$	$\tilde{N} = 51$	$\tilde{N} = 41$	$\tilde{N} = 31$	$\tilde{N} = 26$	$\tilde{N} = 21$	$\tilde{N} = 16$
EndPoint	1.6633	3.2640	5.8730	1.2830	2.6147	4.8714	8.7914	15.5397	24.7731
LinReg	0.0663	0.2705	0.9096	0.0417	0.2111	0.7998	0.4483	1.4320	3.7942
RND	0.0092	0.2456	0.6322	0.0029	0.1974	0.5871	0.0814	1.2084	2.3264
$\Delta K/S_0 = 2\%$	$\tilde{N} = 26$	$\tilde{N} = 21$	$\tilde{N} = 16$	$\tilde{N} = 26$	$\tilde{N} = 21$	$\tilde{N} = 16$	$\tilde{N} = 13$	$\tilde{N} = 11$	$\tilde{N} = 8$
EndPoint	1.6632	3.2638	5.8723	1.2830	2.6145	4.8707	8.7912	15.5392	24.7724
LinReg	0.0695	0.2950	0.9622	0.0440	0.2317	0.8477	0.4672	1.5475	3.9859
RND	0.0247	0.2910	0.7389	0.0138	0.3091	0.6806	0.1767	0.7691	2.7621
$\Delta K/S_0 = 5\%$	$\tilde{N} = 11$	$\tilde{N} = 9$	$\tilde{N} = 7$	$\tilde{N} = 11$	$\tilde{N} = 9$	$\tilde{N} = 7$	$\tilde{N} = 6$	$\tilde{N} = 5$	$\tilde{N} = 4$
EndPoint	1.6631	3.2610	5.8602	1.2830	2.6118	4.8574	8.7869	15.5305	24.7599
LinReg	0.0864	0.3483	1.1026	0.0552	0.2777	0.9750	0.5731	1.7828	4.5043
RND	0.0431	0.2395	0.9310	0.0254	0.2009	0.8484	0.2972	1.1229	3.5479
Panel B: Crisis scenario									
$\Delta K/S_0 = 1\%$	$\tilde{N} = 51$	$\tilde{N} = 41$	$\tilde{N} = 31$	$\tilde{N} = 51$	$\tilde{N} = 41$	$\tilde{N} = 31$	$\tilde{N} = 26$	$\tilde{N} = 21$	$\tilde{N} = 16$
EndPoint	10.0051	12.7713	16.1125	7.1998	9.5509	12.5202	41.4247	48.9762	56.5464
LinReg	2.9197	5.7738	9.3434	1.1772	3.3819	6.8725	16.2173	27.4580	37.6026
RND	1.0707	4.4211	8.2642	0.6228	2.9938	6.0655	5.2882	19.9643	33.5352
$\Delta K/S_0 = 2\%$	$\tilde{N} = 26$	$\tilde{N} = 21$	$\tilde{N} = 16$	$\tilde{N} = 26$	$\tilde{N} = 21$	$\tilde{N} = 16$	$\tilde{N} = 13$	$\tilde{N} = 11$	$\tilde{N} = 8$
EndPoint	10.0047	12.7706	16.1112	7.1996	9.5502	12.5188	41.4237	48.9748	56.5451
LinReg	3.0473	5.9610	9.5065	1.2484	3.5554	7.0111	16.8278	28.0805	38.0727
RND	1.7007	5.0423	8.7383	1.0153	3.4406	6.4392	8.4553	22.5919	35.1688
$\Delta K/S_0 = 5\%$	$\tilde{N} = 11$	$\tilde{N} = 9$	$\tilde{N} = 7$	$\tilde{N} = 11$	$\tilde{N} = 9$	$\tilde{N} = 7$	$\tilde{N} = 6$	$\tilde{N} = 5$	$\tilde{N} = 4$
EndPoint	9.9999	12.7595	16.0892	7.1961	9.5403	12.4954	41.4049	48.9490	56.5220
LinReg	3.3686	6.4980	9.9807	1.3856	4.0447	7.4078	18.4582	29.8796	39.4845
RND	2.5009	5.9561	9.4676	1.4991	4.1168	7.0251	12.4445	26.2664	37.5623

Note: The table shows percentage errors $100 \times |\widehat{\mathcal{Y}} - \mathcal{Y}_{\text{dense}}|/\mathcal{Y}_{\text{dense}}$ for $\mathcal{Y} = \mathbb{V}, \mathbb{IV}, \mathbb{RIX}$ using endpoint volatility (EndPoint), linear regression (LinReg), and RND-tail (RND) extrapolation for the base case (Panel A) and crisis scenario (Panel B). $\mathcal{Y}_{\text{dense}}$ is the respective benchmark computed from the full range of SVCJ OTM option prices $K_{\text{put}}/S_0 \in [0.01, 1]$, $K_{\text{call}}/S_0 \in [1, 1.99]$ ($\mathbb{RIX}$ from OTM put options only), and $\widehat{\mathcal{Y}}$ is the estimate from the truncated and extrapolated volatility smile. Errors are shown for observable moneyness ranges $[K_{\text{put}}^{\min}/S_0, K_{\text{call}}^{\max}/S_0]$ of [0.75, 1.25] (±25%), [0.8, 1.2] (±20%), and [0.85, 1.15] (±15%), where $\mathbb{RIX}$ uses OTM put options only. $\mathcal{Y}_{\text{dense}}$ follow from trapezoidal integration across dense grids of strikes with $\Delta K/S_0 = 0.1\%$. $\widehat{\mathcal{Y}}$ are obtained by assuming that options are available for strike grids with $\Delta K/S_0 = 1\%, 2\%, 5\%$ corresponding to $\tilde{N}$ available contracts which are interpolated by a natural cubic spline to achieve $\Delta K/S_0 = 0.1\%$.

Abbreviations: OTM, out-of-the-money; RND, risk-neutral return distribution; SVCJ, stochastic volatility and contemporaneous jump.

regression, and RND-tail extrapolation. In a first step, cubic spline smoothing is applied to recover a dense grid of strikes with $\Delta K/S_0 = 0.1\%$ from the perturbed implied volatilities. We use the standard cubic smoothing spline for endpoint volatility and linear extrapolation. For RND-tail modeling, we enforce the additional convexity-preserving constraints. The benchmark estimates $\mathcal{Y}_{\text{dense}}$ remain unchanged.

Without noise, estimation errors from endpoint volatility are generally higher than those from the other extrapolation techniques. With noise, they increase only slightly and error standard deviations grow moderately with θ. Simulated microstructure noise mainly affects linear regression and RND-tail extrapolation. In the base case, estimation errors from LinReg rise considerably on average compared with their RND counterparts, even though they

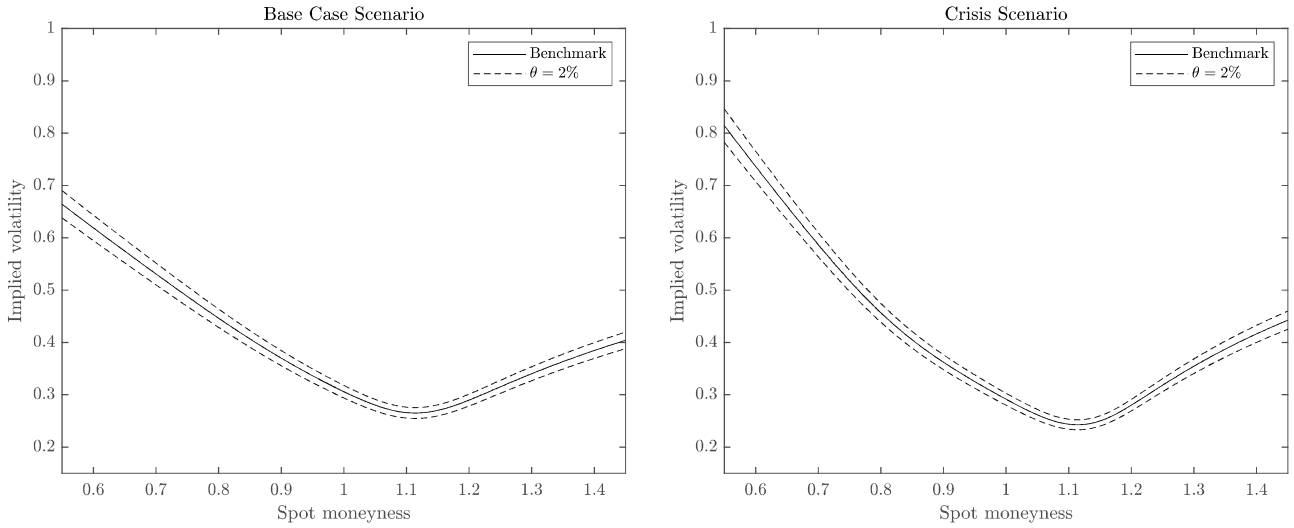

FIGURE 2 Confidence intervals simulated microstructure noise. The figure plots Black and Scholes (1973) implied volatility smiles in the base case (left panel) and crisis scenario (right panel) alongside with the 95% confidence intervals for randomly perturbed observations $\tilde{\sigma}_{\text{noisy},i} = \tilde{\sigma}_i(1 + \theta\eta)$, $i = 1, ..., \tilde{N}$, where $\tilde{\sigma}_i$ are the benchmark implied volatilities generated by the SVCJ model and $\eta \sim \mathcal{N}(0, 1)$ for $\theta = 2\%$. The base case scenario emerges for $\kappa = 1.1521$, $\theta = 0.3437$, $\sigma = 0.6772$, $\rho = -0.5882$, $V_t = 0.0845$, $\lambda = 3.2642$, $\mu_X = -0.0318$, $\sigma_X = 0.0273$, $\mu_y = 0.2245$, and $\rho_J = -0.0921$. The crisis scenario differs in that $\kappa = 1.4333$, $\theta = 0.3779$, $\sigma = 0.9892$, $\rho = -0.6993$, $V_t = 0.0669$, $\lambda = 0.1876$, $\mu_X = 0.0473$, $\sigma_X = 0.2295$, $\mu_y = 0.3962$, and $\rho_J = -0.6677$. Dense-grid estimates of the risk-neutral BKM annualized variance, skewness, and kurtosis are $\text{Var}^{\mathbb{Q}}/T = 0.1116$, $\text{Skew}^{\mathbb{Q}} = -1.1993$, and $\text{Kurt}^{\mathbb{Q}} = 6.5872$ in the base case and $\text{Var}^{\mathbb{Q}}/T = 0.1157$, $\text{Skew}^{\mathbb{Q}} = -2.4563$, and $\text{Kurt}^{\mathbb{Q}} = 19.7374$ in the crisis scenario. BKM, Bakshi, Kapadia, and Madan; SVCJ, stochastic volatility and contemporaneous jump.

do not exceed those from endpoint volatility. Smiles based on linear regression generate the least stable results. In terms of the errors' standard deviation, values are up to 201% for $\Delta K/S_0 = 2\%$ and 20% moneyness range in the case of the $\mathbb{RIX}$, while RND values are moderate. Differences in extrapolation techniques are even more pronounced in the crisis scenario. $\mathbb{RIX}$ estimation errors from EndPoint remain stable but are considerably larger than their LinReg and RND counterparts. LinReg again generates the least stable results now with a standard deviation up to 224% for $\Delta K/S_0 = 2\%$ and 20% moneyness range in the case of the $\mathbb{RIX}$.

The large variations in LinReg error standard deviations in the presence of microstructure noise are due to two contrary effects. First, an unfavorably perturbed implied volatility near the spline's boundary can have a substantial impact on the slope between its outermost knots. Large deviations in this slope and thus estimation errors become more likely. Second, the larger the strike spacing is, the more pronounced is the impact of smoothing. The influence of a single unfavorably perturbed implied volatility near the boundary of the spline can be dampened by the roughness penalty term. As implied volatilities are perturbed randomly, it is difficult to assess which effect will eventually prevail. With the noise level increasing, extreme LinReg errors and error standard deviations become more likely. As already stated by Ammann and Feser (2019), for example, linear extrapolation must be considered as highly unreliable in the presence of microstructure noise. As this technique may yield misleading results, it should not be used in smile construction for the estimation of tail risk metrics, like, the $\mathbb{RIX}$.

Our results show that RND-tail extrapolation is considerably more robust with respect to microstructure noise than linear extrapolation which can be attributed to its construction based on option prices *and* risk-neutral PDF and CDF values. This approach prevents large errors by ensuring that the underlying RND is well-behaved in the sense that it is positive and continuous. Average $\mathbb{RIX}$ estimation errors and standard deviations are generally low. In line with intuition, they increase in the level of the noise. For high microstructure noise and a narrow moneyness range of ⁻15% the advantage of RND-tail modeling over endpoint volatility vanishes with coefficients of variation around 1. In these limiting cases, endpoint volatility may be preferable as it represents the best estimate in the absence of reliable information (e.g., the number of contracts available to smile construction is limited to 4 for $\Delta K/S_0 = 5\%$). This may explain why endpoint volatility is often considered as the method of choice in smile construction. In the crisis scenario, average estimation errors from RND-tail extrapolation are considerably smaller than those from endpoint volatility and error standard deviations remain moderate. RND-tail extrapolation can mitigate the bias induced by endpoint volatility

TABLE 4 Average estimation errors $\mathbb{V}, \mathbb{IV}, \mathbb{RIX}$—Microstructure noise ($\theta = 2\%$).

	$\mathbb{V}$			$\mathbb{IV}$			$\mathbb{RIX}$		
Observable range	**±25%**	**±20%**	**±15%**	**±25%**	**±20%**	**±15%**	**−25%**	**−20%**	**−15%**
Panel A: Base case scenario									
$\Delta K/S_0 = 1\%$									
EndPoint	1.7245	3.2877	5.9337	1.3490	2.6371	4.9308	8.8799	15.5541	24.9031
	(0.7460)	(0.7601)	(0.8481)	(0.6949)	(0.7281)	(0.8034)	(1.6524)	(1.7527)	(2.0070)
LinReg	0.9436	2.1004	3.3834	0.8441	1.6344	2.7139	4.1488	12.1014	17.3491
	(1.0575)	(7.3974)	(10.4656)	(1.3565)	(4.6544)	(6.8053)	(5.4505)	(60.3711)	(83.3280)
RND	0.7662	1.1462	2.0278	0.6740	0.9419	1.6808	3.0339	5.3631	9.1444
	(0.6299)	(1.2992)	(2.0306)	(0.5375)	(0.9245)	(1.4893)	(3.0201)	(8.7003)	(12.2417)
$\Delta K/S_0 = 2\%$									
EndPoint	1.7788	3.2987	5.9019	1.4277	2.6477	4.8977	8.9102	15.6057	24.8691
	(0.9631)	(1.0605)	(1.2002)	(0.8755)	(1.0158)	(1.1445)	(2.2484)	(2.2933)	(2.6485)
LinReg	1.4303	2.6492	3.4581	1.2488	2.0618	2.8319	6.7282	16.5746	16.5630
	(2.7344)	(20.3827)	(5.2640)	(2.0027)	(10.7220)	(3.8991)	(20.2345)	(200.9856)	(33.4848)
RND	1.0566	1.3959	2.4659	0.9341	1.1659	2.0152	4.2326	6.4565	11.4825
	(0.9705)	(1.3217)	(2.7167)	(0.7778)	(1.0112)	(1.9238)	(5.5587)	(7.6908)	(17.5472)
$\Delta K/S_0 = 5\%$									
EndPoint	2.0388	3.3801	5.9434	1.7509	2.7699	4.9194	9.0061	15.5989	25.1786
	(1.3825)	(1.6539)	(1.7790)	(1.2689)	(1.5424)	(1.7348)	(3.2634)	(3.3998)	(3.3091)
LinReg	1.6892	2.1283	2.8492	1.5738	1.8471	2.3821	6.2011	9.5201	12.4604
	(1.4931)	(1.9624)	(2.4454)	(1.3518)	(1.6141)	(1.9505)	(8.4019)	(11.0144)	(12.5932)
RND	1.5129	1.8935	2.5271	1.3856	1.6249	2.1231	5.3290	8.2590	11.2687
	(1.2010)	(1.5731)	(2.2236)	(1.0865)	(1.3023)	(1.7610)	(5.4967)	(8.0713)	(12.0881)
Panel B: Crisis Scenario									
$\Delta K/S_0 = 1\%$									
EndPoint	10.1264	12.8370	16.1891	7.3151	9.6159	12.5958	41.5612	49.0403	56.6415
	(0.7565)	(0.7359)	(0.7966)	(0.7355)	(0.7179)	(0.7751)	(1.2707)	(1.1748)	(1.2229)
LinReg	5.5353	9.3647	11.7996	3.3473	6.4165	8.7549	27.8110	42.8380	47.6512
	(15.6522)	(18.8217)	(17.2233)	(8.3927)	(11.1471)	(10.5816)	(99.1038)	(108.0739)	(94.4738)
RND	4.5607	6.8721	9.7103	3.0284	4.8884	7.2571	20.9241	29.1939	37.9253
	(2.1024)	(2.8439)	(3.7165)	(1.4859)	(2.0446)	(2.6680)	(9.4762)	(12.3837)	(16.1471)
$\Delta K/S_0 = 2\%$									
EndPoint	10.1405	12.8401	16.1573	7.3334	9.6192	12.5632	41.5029	49.0343	56.6007
	(1.0207)	(1.0119)	(1.1160)	(0.9953)	(0.9975)	(1.0953)	(1.6892)	(1.5094)	(1.5849)
LinReg	7.3170	9.3258	10.7803	4.6906	6.5702	8.0290	36.7359	43.4754	42.2453
	(18.2264)	(34.6330)	(6.4968)	(10.5451)	(18.2972)	(4.7217)	(109.5680)	(223.6443)	(27.8208)
RND	4.7910	6.9982	9.4720	3.2182	4.9696	7.0668	21.7683	29.7649	37.0732
	(2.3549)	(3.1150)	(3.7455)	(1.6966)	(2.2556)	(2.8052)	(10.4324)	(13.5568)	(15.1840)

(Continues)

TABLE 4 (Continued)

	$\mathbb{V}$			$\mathbb{IV}$			$\mathbb{RIX}$		
Observable range	**±25%**	**±20%**	**±15%**	**±25%**	**±20%**	**±15%**	**−25%**	**−20%**	**−15%**
$\Delta K/S_0 = 5\%$									
EndPoint	10.1426	12.8611	16.1838	7.3377	9.6483	12.5722	41.4850	48.9443	56.7468
	(1.6413)	(1.5928)	(1.6389)	(1.6317)	(1.5876)	(1.6504)	(2.3303)	(2.1869)	(1.9497)
LinReg	5.3366	6.9507	10.0354	3.7445	4.7684	7.5110	25.7046	30.4975	38.9435
	(4.7442)	(4.0461)	(3.6064)	(3.6374)	(3.0914)	(2.9649)	(22.4480)	(16.7320)	(11.3941)
RND	5.0353	6.8641	9.7635	3.4331	4.9098	7.3054	22.8725	28.8523	37.9672
	(2.7462)	(3.5065)	(3.3383)	(2.0259)	(2.5905)	(2.7144)	(11.9799)	(14.7157)	(11.2561)

Note: The table shows simulation-based averages (1000 runs) of percentage errors $100 \times |\widehat{\mathcal{Y}} - \mathcal{Y}_{\text{dense}}|/\mathcal{Y}_{\text{dense}}$ for $\mathcal{Y} = \mathbb{V}, \mathbb{IV}, \mathbb{RIX}$ using endpoint volatility (EndPoint), linear regression (LinReg), and RND-tail (RND) extrapolation for the base case (Panel A) and crisis scenario (Panel B) with error standard deviation in parentheses. $\mathcal{Y}_{\text{dense}}$ is the respective benchmark computed from the full range of SVCJ OTM option prices $K_{\text{put}}/S_0 \in [0.01, 1]$, $K_{\text{call}}/S_0 \in [1, 1.99]$ ($\mathbb{RIX}$ OTM put options only) using trapezoidal integration over dense grids of strikes with $\Delta K/S_0 = 0.1\%$. Estimates $\widehat{\mathcal{Y}}$ are obtained from randomly perturbed implied volatility smiles $\tilde{\sigma}_{\text{noisy},i} = \tilde{\sigma}_i(1 + 0.02\eta)$, $i = 1, ..., \tilde{N}$, where $\tilde{\sigma}_i$ are Black and Scholes (1973) implied volatilities computed from SVCJ option prices and $\eta \sim \mathcal{N}(0, 1)$. $\widehat{\mathcal{Y}}$ are computed from extrapolated moneyness ranges $[K_{\text{put}}^{\min}/S_0, K_{\text{call}}^{\max}/S_0]$ of [0.75, 1.25] (±25%), [0.8, 1.2] (±20%), and [0.85, 1.15] (±15%) ($\mathbb{RIX}$: OTM put options only) based on cubic spline smoothing (RND: with convexity constraints) of strike grids with $\Delta K/S_0 = 1\%, 2\%, 5\%$.

Abbreviations: OTM, out-of-the-money; RND, risk-neutral return distribution; SVCJ, stochastic volatility and contemporaneous jump.

and is—at the same time—considerably more stable than linear extrapolation. In particular when event risk is high, it is the superior approach to obtain accurate estimates of the $\mathbb{RIX}$ and similar metrics.

5 | EMPIRICAL APPLICATION

In this section, we empirically analyze the RND-based smile construction approach and outline its impact on $\mathbb{RIX}$ estimates for a normal and a volatile trading day. First, we compare the efficiency of the RND-based technique to that of standard approaches by constructing volatility smiles based on narrowed moneyness ranges. To assess the accuracy of the different smile construction approaches, discarded contracts are used to compute the RMSE of extrapolated implied volatilities. Second, we estimate the $\mathbb{RIX}$ based on the full set of observable *and* constructed OTM put options. Section 5.1 details the data and the estimation approach, the main results are given in Section 5.2.

5.1 | Data and summary statistics

Analogous to the base case and crisis scenario in the numerical analysis, we identify a normal (May 22, 2019) and a volatile trading day (May 20, 2020). While the normal day is characterized by a VIX level of 15, the volatile day lies within the COVID pandemic and exhibits a VIX level of 28. To obtain a sufficient number of observable contracts for our analysis, we focus on 30-day quarterly options written on the highly liquid stocks of *FAANG* stocks.[19] This ensures that the number of OTM option contracts is sufficiently large to compute meaningful RMSE. Raw options data are obtained from the OptionMetrics database which also provides European options that are calculated from American options. Table 5 shows summary statistics for implied volatilities of *FAANG* individual stock options for both observation dates. Almost all moments exhibit higher values on the volatile day. The ratio of mean and median indicates a right-skewed distribution of implied volatilites for both days.

Table 6 conveys information about the number of OTM contracts available in moneyness intervals of 0.05. The number of OTM put options with a spot moneyness less than 0.75 is substantially higher on the volatile than on the

[19] *FAANG* stocks did not pay any dividends within the periods under consideration.

TABLE 5 Summary statistics—Implied volatilities.

	Mean	SD	Median	Min	Max
Panel A: May 22, 2019 (normal)					
AAPL	0.4380	0.1337	0.4377	0.2656	0.8937
AMZN	0.4003	0.2477	0.2915	0.2205	1.3737
FB	0.4538	0.2707	0.3435	0.2160	1.2937
GOOG	0.3410	0.1893	0.2763	0.1840	1.0376
NFLX	0.5360	0.2945	0.3991	0.2855	1.4177
Panel B: May 20, 2020 (volatile)					
AAPL	0.5939	0.3758	0.4500	0.2379	1.7140
AMZN	0.5380	0.2767	0.4429	0.2850	1.4074
FB	0.5693	0.2556	0.4594	0.3387	1.2458
GOOG	0.5330	0.2917	0.4320	0.2190	1.2514
NFLX	0.8303	0.6023	0.5682	0.3759	2.8537

Note: The table shows mean, standard deviation (SD), median, minimum (Min), and maximum (Max) for implied volatilities of 30-day quarterly options written on the *FAANG* stocks (Facebook [FB] [Meta], Amazon [AMZN], Apple [AAPL], Netflix [NFLX], Google [GOOG] [Alphabet]) on May 22, 2019 (Panel A, normal) and May 20, 2020 (Panel B, volatile). Data are retrieved from OptionMetrics and individual stocks are identified by their ticker symbols.

normal day. This reflects the fact that these contracts are often used as "crash insurances" in volatile market conditions.

5.2 | Results

We apply RND-tail extrapolation, endpoint volatility, and linear regression combined with cubic spline smoothing (RND with convexity constraints) to construct full volatility smiles for moneyness ranges around the spot of ±25%, ±20%, and ±15%, respectively. For OTM put options, we compute RMSE of extrapolated implied volatilities with respect to their observable counterparts located outside the respective moneyness range. We compare the accuracy of the different smile extrapolation techniques in the relevant domain for capturing rare disaster concerns. $\mathbb{RIX}$ estimates are then computed from the set of observable *and* constructed OTM put option prices.

Table 7 shows the results. First, RMSEs of implied volatilities based on the RND approach are substantially smaller than those based on standard techniques. This holds for all *FAANG* stocks and all three moneyness ranges on both trading days. On average, RMSE of extrapolated volatilities differs between the RND approach and endpoint volatility (linear regression) by 0.27 (0.05) for the normal and 0.37 (0.07) for the volatile day. Furthermore, RMSE is robust with respect to the size of the available moneyness range with similar orders of magnitude. This indicates that RND-tail extrapolation is superior to endpoint volatility and linear regression when brought to the data. Figure 3 illustrates the differences in smile construction for Apple and Google on the normal and the volatile trading day. Discarded implied volatilities from OTM put options are more accurately matched by the RND-based approach than by its competitors. The improvement is even more pronounced for the volatile trading day indicating that RND-based smile construction is particularly advantageous when rare disaster concerns may be present.

Second, RND-based $\mathbb{RIX}$ estimates on the volatile day are considerably higher than those from standard techniques. This holds across all *FAANG* stocks and all three moneyness ranges. On average, estimates using the RND approach exceed those from endpoint volatility (linear regression) by 0.0033 (0.0012) in absolute and 73.97% (18.29%) in relative terms on that day. For the normal day, the differences are less pronounced. On average, RND-based $\mathbb{RIX}$ estimates still exceed those from endpoint volatility (linear regression) by 0.0010

TABLE 6 Summary statistics—Number of OTM option contracts.

	OTM put options						OTM call options					
Moneyness	**0–0.75**	**0.75–0.80**	**0.80–0.85**	**0.85–0.90**	**0.90–0.95**	**0.95–1.00**	**1.00–1.05**	**1.05–1.10**	**1.10–1.15**	**1.15–1.20**	**1.20–1.25**	**1.25–∞**
Panel A: May 22, 2019 (normal)												
AAPL	18	9	6	3	4	4	3	4	4	2	2	19
AMZN	84	15	13	18	19	26	37	19	18	15	13	35
FB	17	2	2	3	4	4	3	4	3	2	2	12
GOOG	30	12	11	12	11	22	23	13	6	6	5	25
NFLX	35	4	4	3	6	7	8	5	3	4	3	25
Panel B: May 20, 2020 (volatile)												
AAPL	33	4	3	4	7	6	5	3	3	3	3	12
AMZN	135	25	25	25	25	22	13	8	6	6	8	30
FB	21	3	5	4	5	4	3	2	2	3	2	8
GOOG	102	9	14	14	14	14	14	14	7	7	7	15
NFLX	60	4	5	4	5	4	5	4	4	5	4	27

Note: The table shows the number of out-of-the-money (OTM) 30-day quarterly option contracts written on the *FAANG* stocks (Facebook [FB] [Meta], Amazon [AMZN], Apple [AAPL], Netflix [NFLX], Google [GOOG] [Alphabet]) on May 22, 2019 (Panel A, normal) and May 20, 2020 (Panel B, volatile) for moneyness intervals of 0.05. Data are obtained from OptionMetrics and individual stocks are identified by their ticker symbols.

TABLE 7 RMSE and $\mathbb{RIX}$ estimates.

	Panel A: May 22, 2019 (normal)						Panel B: May 20, 2020 (volatile)					
	RMSE			$\widehat{\mathbb{RIX}}$			RMSE			$\widehat{\mathbb{RIX}}$		
Observable range	−25%	−20%	−15%	−25%	−20%	−15%	−25%	−20%	−15%	−25%	−20%	−15%
AAPL												
EndPoint	0.1631	0.1585	0.1757	0.0052	0.0048	0.0041	0.5489	0.5822	0.6050	0.0063	0.0051	0.0041
LinReg	0.0471	0.0382	0.0492	0.0058	0.0058	0.0053	0.1729	0.1862	0.1932	0.0100	0.0091	0.0086
RND	0.0383	0.0295	0.0389	0.0058	0.0059	0.0053	0.0906	0.0858	0.0809	0.0118	0.0114	0.0113
AMZN												
EndPoint	0.3925	0.3981	0.4108	0.0026	0.0023	0.0020	0.4103	0.4246	0.4361	0.0037	0.0032	0.0028
LinReg	0.1634	0.1492	0.1558	0.0029	0.0029	0.0027	0.1205	0.1269	0.1628	0.0051	0.0047	0.0040
RND	0.0927	0.0786	0.0851	0.0030	0.0030	0.0028	0.0526	0.0646	0.0769	0.0084	0.0058	0.0049
FB												
EndPoint	0.4231	0.4452	0.4695	0.0029	0.0025	0.0021	0.4249	0.4318	0.4249	0.0064	0.0059	0.0052
LinReg	0.1542	0.1234	0.1632	0.0033	0.0035	0.0030	0.1612	0.1826	0.2459	0.0076	0.0072	0.0063
RND	0.0791	0.0533	0.0783	0.0035	0.0037	0.0031	0.1136	0.1276	0.2331	0.0078	0.0074	0.0064
GOOG												
EndPoint	0.3178	0.3102	0.3129	0.0017	0.0015	0.0013	0.3861	0.4180	0.4416	0.0042	0.0036	0.0030
LinReg	0.0944	0.0894	0.0919	0.0022	0.0021	0.0020	0.1330	0.1186	0.1424	0.0057	0.0059	0.0050
RND	0.0643	0.0545	0.0584	0.0025	0.0024	0.0022	0.0898	0.0682	0.0856	0.0066	0.0077	0.0061
NFLX												
EndPoint	0.4693	0.4944	0.5109	0.0050	0.0044	0.0037	0.9903	0.9967	0.9968	0.0072	0.0065	0.0056
LinReg	0.1535	0.1880	0.2433	0.0063	0.0057	0.0050	0.5626	0.6122	0.7448	0.0097	0.0086	0.0068
RND	0.0815	0.1128	0.1796	0.0066	0.0058	0.0050	0.3303	0.3806	0.7436	0.0106	0.0091	0.0068

Note: The table shows RMSE of extrapolated implied volatilities with respect to observable discarded OTM put options written on the *FAANG* stocks (Facebook [FB] [Meta], Amazon [AMZN], Apple [AAPL], Netflix [NFLX], Google [GOOG] [Alphabet]) for May 22, 2019 (Panel A, normal) and May 20, 2020 (Panel B, volatile). Volatility smiles are constructed using endpoint volatility (EndPoint), linear regression (LinReg), and RND-tail (RND) extrapolation combined with cubic spline smoothing (RND with convexity constraints) based on narrowed moneyness ranges $[K_{\text{put}}^{\min}/S_0, K_{\text{call}}^{\max}/S_0]$ of [0.75, 1.25] (±25%), [0.8, 1.2] (±20%), and [0.85, 1.15] (±15%). RMSE and $\widehat{\mathbb{RIX}}$ follow from OTM put options only which are indicated by the negative sign of the underlying moneyness range. We compute $\widehat{\mathbb{RIX}}$ from a dense grid of observable *and* constructed OTM put option prices using trapezoidal integration. ΔK is chosen such that observable strikes are included as knots while ensuring $\Delta K/S_0 \leq 0.1\%$. Individual stocks are identified by their ticker symbols.

Abbreviations: OTM, out-of-the-money; RMSE, root mean square error; RND, risk-neutral return distribution.

(0.0001) in absolute and 35.59% (4.87%) in relative terms. Given the higher accuracy of RND-tail extrapolation, we conclude that corresponding $\mathbb{RIX}$ estimates are superior to their counterparts from standard techniques. Endpoint volatility and linear regression tend to underestimate rare disaster concerns when jump and tail risks are prevalent.

This is further illustrated by aligning the volatility smiles of Apple and Google in Figure 3 with the corresponding $\mathbb{RIX}$ estimates in Table 7. On both observation days, RND-based extrapolated volatility smiles exhibit curvature and clearly differ from those using endpoint volatility and linear regression. This only translates to substantial differences in $\mathbb{RIX}$ estimates on the volatile day, though. RND-tail modeling takes curvature into account explicitly. This additional flexibility allows one to incorporate higher implied volatilities of far OTM put options. When market volatility is high, these contracts tend to be more expensive than on days with moderate volatility. As far OTM puts influence $\mathbb{RIX}$ estimates substantially due to the implicit weighting scheme in (8), small changes in their prices have a comparably large impact.

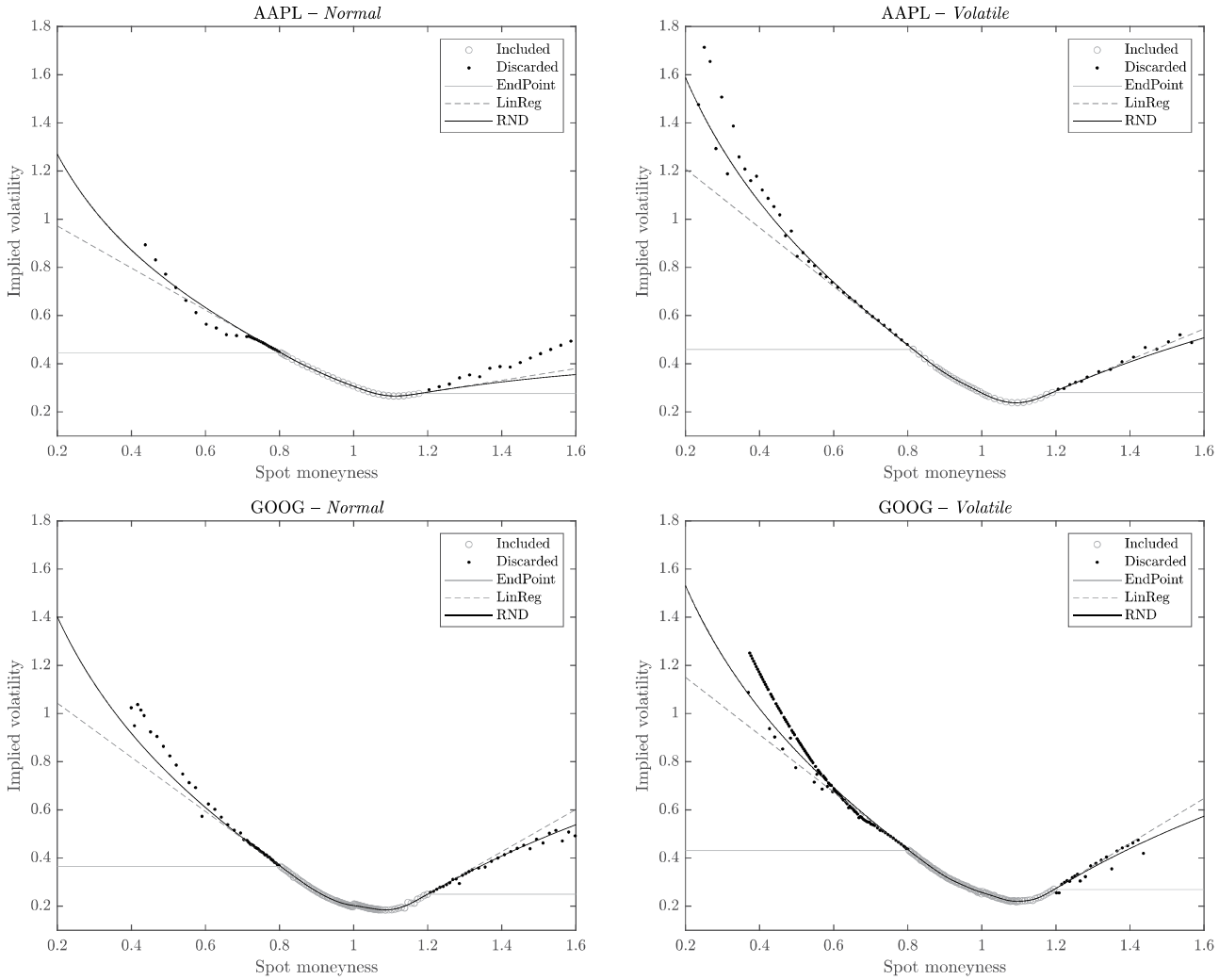

FIGURE 3 Empirical extrapolated volatility smiles. The figure plots extrapolated Black and Scholes (1973) implied volatility smiles for option contracts on Apple (AAPL, top panels) and Google (GOOG, bottom panels) on the normal (left panels) and the volatile observation day (right panels). On the basis of implied volatilities of observable contracts in a narrowed spot moneyness range of [0.80, 1.20] ("Included"), volatility smiles are extrapolated by endpoint volatility (EndPoint), linear regression (LinReg), and RND-tail (RND) extrapolation after cubic spline smoothing (RND with convexity constraints). Implied volatilities of observable contracts outside the moneyness range ("Discarded") are plotted against extrapolated volatility smiles. Options data are obtained from OptionMetrics.

6 | CONCLUSION

In this paper we develop a new arbitrage-free RND-based smile construction approach. Our main goal is to improve the accuracy and stability of estimators of model-free event risk measures, like, the rare disaster concern index $\mathbb{RIX}$ (Gao et al., 2018, 2019). These are commonly defined for a continuum of strike prices that is not available in practice. Thus, numerical approximation techniques must be applied. As metrics like the $\mathbb{RIX}$ significantly depend on deep OTM options, biases induced by standard extrapolation methods can be critical when the underlying RND features high kurtosis and negative skewness. Numerical and empirical analyses confirm that $\mathbb{RIX}$ estimates based on standard techniques are the least accurate when event risk is high—the type of risk this metric is supposed to capture.

Exploiting the one-to-one relation between option prices and the underlying RND, we extrapolate the implied volatility smile by modeling the tails of the RND using the GEV distribution. We then match option prices *and* the RND implied by the GEV tails and observable contracts to obtain the full smile. This new optimization approach ensures that the transition between extrapolated and observable implied volatilities is always continuous. As this requires that the underlying RND is well-behaved, we interpolate observable implied volatilities using a cubic smoothing spline with additional convexity constraints.

The numerical analysis sheds light on how limited moneyness ranges and different strike spacing affect estimation errors in the base case and the crisis scenario. Results from standard techniques are consistent with findings in the literature. We analyze the impact of microstructure noise by performing a simulation study. In contrast to other studies in the literature, we systematically investigate the interplay between different sources of error. It turns out that—due to its flexibility—RND-tail modeling shares the favorable properties of both endpoint volatility and linear extrapolation without being affected by the major shortcomings of its competitors. It (1) substantially reduces the bias in far OTM implied volatilities that are typically induced by endpoint volatility and (2) is considerably more robust to microstructure noise than linear extrapolation.

We empirically verify our findings by looking at options on *FAANG* stocks on a normal and a volatile trading day for narrowed moneyness ranges. RMSE of extrapolated implied volatilities with respect to those of discarded OTM put options show that RND-tail extrapolation matches the data considerably better than standard techniques. For the volatile day, we find that $\mathbb{RIX}$ estimates using the RND approach exceed those from endpoint volatility (linear regression) by 0.0033 (0.0012) on average. Given the added accuracy of the RND approach, we conclude that endpoint volatility and linear regression tend to underestimate rare disaster concerns when jump and tail risks are prevalent.

ACKNOWLEDGMENTS

The research did not receive any specific grant from funding agencies in the public, commercial, or not-for-profit sectors. Open Access funding enabled and organized by Projekt DEAL.

CONFLICT OF INTEREST STATEMENT

The authors declare no conflict of interest.

DATA AVAILABILITY STATEMENT

The data that support the findings of this study are available from OptionMetrics. Restrictions apply to the availability of these data, which were used under license for this study. Retrieving the data requires a subscription to OptionMetrics IvyDB US.

ORCID

Michael Herold http://orcid.org/0000-0003-3361-3869
Matthias Muck http://orcid.org/0000-0003-2364-9833

REFERENCES

Ait-Sahalia, Y., & Lo, A. W. (1998). Nonparametric estimation of state-price densities implicit in financial asset prices. *The Journal of Finance*, *53*, 499–547.

Ammann, M., & Feser, A. (2019). Robust estimation of risk-neutral moments. *Journal of Futures Markets*, *39*, 1137–1166.

Aschakulporn, P., & Zhang, J. E. (2022a). Bakshi, Kapadia, and Madan (2003) risk-neutral moment estimators: A Gram–Charlier density approach. *Review of Derivatives Research*, *25*, 233–281.

Aschakulporn, P., & Zhang, J. E. (2022b). Bakshi, Kapadia, and Madan (2003) risk-neutral moment estimators: An affine jump-diffusion approach. *Journal of Futures Markets*, *42*, 365–388.

Backus, D., Chernov, M., & Martin, I. A. (2011). Disasters implied by equity index options. *The Journal of Finance*, *66*, 1969–2012.

Bahra, B. (1997). *Implied risk-neutral probability density functions from option prices: Theory and application* [Unpublished, Working Paper].

Bakshi, G., Kapadia, N., & Madan, D. (2003). Stock return characteristics, skew laws, and the differential pricing of individual equity options. *Review of Financial Studies*, *16*, 101–143.

Bali, T. G. (2003). The generalized extreme value distribution. *Economics Letters*, *79*, 423–427.

Barro, R. J. (2006). Rare disasters and asset markets in the twentieth century. *The Quarterly Journal of Economics*, *121*, 823–866.

Barro, R. J. (2009). Rare disasters, asset prices, and welfare costs. *American Economic Review*, *99*, 243–264.

Bates, D. S. (1996). Jumps and stochastic volatility: Exchange rate processes implicit in Deutsche Mark options. *Review of Financial Studies*, *9*, 69–107.

Birru, J., & Figlewski, S. (2012). Anatomy of a meltdown: The risk neutral density for the S&P 500 in the fall of 2008. *Journal of Financial Markets*, *15*, 151–180.

Black, F., & Scholes, M. (1973). The pricing of options and corporate liabilities. *The Journal of Political Economy*, *81*, 637–654.

Bliss, R. R., & Panigirtzoglou, N. (2002). Testing the stability of implied probability density functions. *Journal of Banking & Finance*, *26*, 381–422.

Bollerslev, T., Gibson, M., & Zhou, H. (2011). Dynamic estimation of volatility risk premia and investor risk aversion from option-implied and realized volatilities. *Journal of Econometrics*, *160*, 235–245.

Breeden, D. T., & Litzenberger, R. H. (1978). Prices of state-contingent claims implicit in option prices. *The Journal of Business*, *51*, 621–651.
Britten-Jones, M., & Neuberger, A. (2000). Option prices, implied price processes, and stochastic volatility. *The Journal of Finance*, *55*, 839–866.
Brunner, B., & Hafner, R. (2003). Arbitrage-free estimation of the risk-neutral density from the implied volatility smile. *The Journal of Computational Finance*, *7*, 75–106.
Carr, P., & Madan, D. (1998). Towards a theory of volatility trading. In R. A. Jarrow (Ed.), *Volatility* (pp. 417–427). Risk Books.
Carr, P., & Wu, L. (2009). Variance risk premiums. *Review of Financial Studies*, *22*, 1311–1341.
Demeterfi, K., Derman, E., Kamal, M., & Zou, J. (1999). A guide to volatility and variance swaps. *The Journal of Derivatives*, *6*, 9.
Dennis, P., & Mayhew, S. (2009). Microstructural biases in empirical tests of option pricing models. *Review of Derivatives Research*, *12*, 169–191.
Dole, D. (1999). CoSmo: A constrained scatterplot smoother for estimating convex, monotonic transformations. *Journal of Business & Economic Statistics*, *17*, 444–455.
Duffie, D., Pan, J., & Singleton, K. (2000). Transform analysis and asset pricing for affine jump-diffusions. *Econometrica*, *68*, 1343–1376.
Eriksson, A., Ghysels, E., & Wang, F. (2009). The normal inverse Gaussian distribution and the pricing of derivatives. *The Journal of Derivatives*, *16*, 23.
Fengler, M. R. (2009). Arbitrage-free smoothing of the implied volatility surface. *Quantitative Finance*, *9*, 417–428.
Figlewski, S. (2018). Risk-neutral densities: A review. *Annual Review of Financial Economics*, *10*, 329–359.
Gao, G. P., Gao, P., & Song, Z. (2018). Do hedge funds exploit rare disaster concerns? *Review of Financial Studies*, *31*, 2650–2692.
Gao, G. P., Lu, X., & Song, Z. (2019). Tail risk concerns everywhere. *Management Science*, *65*, 3111–3130.
Green, P. J., & Silverman, B. W. (1994). Nonparametric regression and generalized linear models: A roughness penalty approach. In D. R. Cox, D. V. Hinkley, N. Keiding, N. Reid, D. B. Rubin, & B. W. Silverman (Eds.), *Monographs on statistics and applied probability* (Vol. 58, 1st ed.). Chapman & Hall.
Jiang, G. J., & Tian, Y. S. (2005). The model-free implied volatility and its information content. *Review of Financial Studies*, *18*, 1305–1342.
Jiang, G. J., & Tian, Y. S. (2007). Extracting model-free volatility from option prices. *The Journal of Derivatives*, *14*, 35–60.
Kapadia, N., & Du, J. (2012). *The tail in the volatility index* [Unpublished, Working Paper].
Muck, M. (2022). Arbitrage-free smile construction on FX option markets using Garman–Kohlhagen deltas and implied volatilities. *Review of Derivatives Research*, *25*, 293–314.
Seo, S. B., & Wachter, J. A. (2019). Option prices in a model with stochastic disaster risk. *Management Science*, *65*, 3449–3469.
Shimko, D. (1993). Bounds of probability. *Risk*, *6*, 33–37.
Wachter, J. A. (2013). Can time-varying risk of rare disasters explain aggregate stock market volatility? *The Journal of Finance*, *68*, 987–1035.

How to cite this article: Albert, P., Herold, M., & Muck, M. (2023). Estimation of rare disaster concerns from option prices—An arbitrage-free RND-based smile construction approach. *The Journal of Futures Markets*, *43*, 1807–1835. https://doi.org/10.1002/fut.22457

APPENDIX A

A.1 | GEV distribution

The GEV distribution follows from the Fisher–Tippett–Gnedenko theorem. Assume that for a sequence of i.i.d. random variables $(X_i)_{i\in\mathbb{N}_0}$ with maximum $M_n = \max\{X_1, ..., X_n\}$ there exist sequences of constants a_n, b_n with $a_n > 0$ such that the normalized maximum converges in distribution to some nondegenerate random variable:

$$\frac{M_n - b_n}{a_n} \xrightarrow{d} X^*.$$

Then, this random variable follows a GEV distribution, $X^* \sim GEV(\mu, \sigma, \xi)$. Its three parameters control location (μ), scale (σ), and shape (ξ). The corresponding PDF $f_{GEV}(x)$ and CDF $F_{GEV}(x)$ are given by

$$f_{GEV}(x) = \frac{1}{\sigma} t(x)^{\xi+1} \exp\{-t(x)\}, \tag{A1}$$

where

$$t(x) = \begin{cases} 1 + \xi\left(\frac{x-\mu}{\sigma}\right)^{-1/\xi} & \text{for } \xi \neq 0, \\ \exp\left\{-\left(\frac{x-\mu}{\sigma}\right)\right\} & \text{for } \xi = 0 \end{cases}$$

and

$$F_{GEV}(x) = \begin{cases} \exp\left\{-\left[1 + \xi\left(\frac{x-\mu}{\sigma}\right)\right]^{-1/\xi}\right\} & \text{for } \xi \neq 0, \\ \exp\left\{-\exp\left\{-\left(\frac{x-\mu}{\sigma}\right)\right\}\right\} & \text{for } \xi = 0. \end{cases} \tag{A2}$$

The support of the distribution varies depending on ξ such that

$$\begin{cases} x \in \left[\mu - \frac{\sigma}{\xi}, +\infty\right) & \text{for } \xi > 0, \\ x \in (-\infty, +\infty) & \text{for } \xi = 0, \\ x \in \left(-\infty, \mu - \frac{\sigma}{\xi}\right] & \text{for } \xi < 0. \end{cases} \tag{A3}$$

A.2 | Cubic smoothing spline with convexity constraints

Consider $i = 1, ..., \tilde{N}$ *observable* implied volatilities $\tilde{\sigma}_i$ with corresponding *observable* strikes $\tilde{K}_i$ ("knots") where $\tilde{K}_1 = K_1$ and $\tilde{K}_{\tilde{N}} = K_N$. A function $g(K)$ is called a natural cubic spline defined on $[\tilde{K}_1, \tilde{K}_{\tilde{N}}]$ if it is a cubic polynomial on every subinterval $[\tilde{K}_i, \tilde{K}_{i+1}]$, if g, g', and g'' are continuous at every knot $\tilde{K}_i$, and if $g'' = g''' = 0$ at $\tilde{K}_1$ and $\tilde{K}_{\tilde{N}}$ (Green & Silverman, 1994). The function g can then be specified by

$$g(K) = a_i + b_i(K - \tilde{K}_i) + c_i(K - \tilde{K}_i)^2 + d_i(K - \tilde{K}_i)^3 \quad \text{for} \tilde{K}_i \leq K \leq \tilde{K}_{i+1}, \tag{A4}$$

where $a_i, b_i, c_i, d_i \in \mathbb{R}$ are given constants. The natural cubic spline incorporates all available data points and is thus suitable for interpolation. If the data are affected by microstructure noise, smoothing is required, though. By incorporating a penalty for curvature which is controlled by the parameter $\lambda > 0$, the cubic smoothing spline results from minimizing

$$\sum_{i=1}^{\tilde{N}} (\tilde{\sigma}_i - g(\tilde{K}_i))^2 + \lambda \int_{\tilde{K}_1}^{\tilde{K}_{\tilde{N}}} g''(K)^2 dK. \tag{A5}$$

The cubic smoothing spline defined by Equation (A5) can be formulated as a quadratic optimization program. Convexity-preserving bounds on the second-order derivatives can be added as additional constraints. Define the $(2\tilde{N} - 2)$-element column vectors $\boldsymbol{y} = (\tilde{\sigma}_1, ..., \tilde{\sigma}_{\tilde{N}}, 0, ..., 0)^\intercal$ and $\boldsymbol{x} = (g_1, ..., g_{\tilde{N}}, \gamma_2, ..., \gamma_{\tilde{N}-1})^\intercal$, where $g_i = g(\tilde{K}_i)$ and $\gamma_i = g''(\tilde{K}_i)$ are the values and second-order derivatives of the spline at the knots $\tilde{K}_i$. The optimization problem then reads

$$\begin{aligned} \underset{\boldsymbol{x}}{\arg\min} \quad & -\boldsymbol{y}^\intercal \boldsymbol{x} + \tfrac{1}{2}\boldsymbol{x}^\intercal \begin{pmatrix} \boldsymbol{I}_{\tilde{N}} & \boldsymbol{0}_{\tilde{N}\times(\tilde{N}-2)} \\ \boldsymbol{0}_{(\tilde{N}-2)\times\tilde{N}} & \lambda \boldsymbol{R} \end{pmatrix} \boldsymbol{x} \\ \text{subject to} \quad & (\boldsymbol{Q}^\intercal - \boldsymbol{R}^\intercal)\boldsymbol{x} = \boldsymbol{0}_{(2\tilde{N}-2)\times 1}, \\ & \gamma_2, \ ..., \ \gamma_{\tilde{N}-1} \geq 0, \end{aligned} \tag{A6}$$

where $\gamma_i \geq 0 \ \ \forall\, i = 2, ..., \tilde{N} - 1$ represents the convexity constraints. $\boldsymbol{I}_n$ is the identity matrix of dimension n and $\boldsymbol{0}_{k\times l}$ is a matrix of zeros with k rows and l columns. The matrices $\boldsymbol{Q} \in \mathbb{R}^{\tilde{N}\times(\tilde{N}-2)}$ and $\boldsymbol{R} \in \mathbb{R}^{(\tilde{N}-2)\times(\tilde{N}-2)}$ are functions in the knots $\tilde{K}_i$.

The elements $q_{i,j}$ of $\boldsymbol{Q}$ are specified using nonstandard indexing with $i = 1, ..., \tilde{N}$ and $j = 2, ..., \tilde{N} - 1$ (e.g., the top left element is $q_{1,2}$ and the bottom right is $q_{\tilde{N},\tilde{N}-2}$). They are given by

$$q_{k-1,k} = h_{k-1}^{-1}, \quad q_{k,k} = -h_{k-1}^{-1} - h_k^{-1}, \quad \text{and} \quad q_{k+1,k} = h_k^{-1} \quad \text{for } k = 2, ..., \tilde{N} - 1, \tag{A7}$$

where $h_i = \tilde{K}_{i+1} - \tilde{K}_i$ and $q_{i,j} = 0$ for $|i - j| \geq 2$. For $\boldsymbol{R}$, the indexing of its elements $r_{i,j}$ is also nonstandard with $i, j = 2, ..., \tilde{N} - 1$. They are given by

$$\begin{aligned} r_{k,k} &= \tfrac{1}{3}(h_{k-1} + h_k) \quad \text{for } k = 2, ..., \tilde{N} - 1, \\ r_{k,k+1} = r_{k+1,k} &= \tfrac{1}{6}h_k \quad \text{for } k = 2, ..., \tilde{N} - 2, \end{aligned} \tag{A8}$$

and $r_{i,j} = 0$ for $|i - j| \geq 2$. $\boldsymbol{R}$ is strictly diagonally dominant and thus positive-definite.

The coefficients of the piecewise polynomial representation in Equation (A4) can be recovered by

$$\begin{aligned} a_i &= g_i, \quad b_i = \tfrac{g_{i+1} - g_i}{h_i} - \tfrac{h_i}{6}(2\gamma_i + \gamma_{i+1}), \\ c_i &= \tfrac{\gamma_i}{2}, \quad d_i = \tfrac{\gamma_{i+1} - \gamma_i}{6h_i}. \end{aligned} \tag{A9}$$

Proofs and technical details are available in Green and Silverman (1994).

The smoothing parameter λ is determined by the "leave-one-out" cross-validation approach.[20] Details on this standard procedure are available in Green and Silverman (1994).[21]

A.3 | SVCJ model and benchmark scenarios

Benchmark model: In the Duffie et al. (2000) affine jump-diffusion model with SVCJs the dynamics of the stock price under the risk-neutral measure $\mathbb{Q}$ are

$$\begin{aligned} \frac{dS_t}{S_t} &= (r - \lambda\mu_X)dt + \sqrt{V_t}dW_t^S + (e^{X_t} - 1)dN_t, \\ dV_t &= \kappa(\theta - V_t)dt + \sigma\sqrt{V_t}dW_t^V + ydN_t - \lambda\mu_y dt, \end{aligned} \tag{A10}$$

where r denotes the constant risk-free interest rate with continuous compounding and V_t the stochastic variance which is driven by a square-root diffusion process with speed κ, long-term mean θ, and diffusive volatility σ. The Brownian motion of the stock price process W_t^S and of the variance W_t^V have correlation ρ. N_t is a Poisson counter with intensity λ. Given the occurrence of a contemporaneous jump, the variance rate jump size y is exponentially distributed with mean μ_y while the price jump size X is normally distributed with mean $\mu_X + \rho_J y$ and variance σ_X, where ρ_J denotes the jump sizes correlation. The model's implementation is based on the characteristic function of log returns as described in Aschakulporn and Zhang (2022b).

Benchmark scenarios: Table A1 states the parametrizations to create a base case and a crisis scenario. Parameters result from model calibration on Apple's quarterly stock options with 30 days to expiration on two trading days. The normal trading day (May 22, 2019) is characterized by a VIX level of 15 and is used for the base case scenario, while the volatility trading day (May 20, 2020) exhibits a VIX level of 28 and refers to the crisis scenario. The error metric applied for calibration is the relative RMSE. Spot price and risk-free interest rate are chosen arbitrarily ($S_t = 100$, $r = 0.02$).

A.4 | Birru and Figlewski (2012) tail-modeling approach

We compare the tail-modeling approach of Birru and Figlewski (2012) to the RND-tail extrapolation with respect to modeled RND tails, volatility smile's continuity, and $\mathbb{RIX}$ estimates. For the crisis scenario and a spot moneyness range

[20]The minimization of the cross-validation score is carried out using the derivative-free Matlab solver patternsearch.

[21]Fengler (2009) states that "leave-one-out" cross-validation is not applicable in his setting. This is mainly due to the focus on the construction of the entire volatility surface. As we limit our analysis to the cross section of strikes for a specific maturity, the parameter λ can be chosen optimally using the aforementioned technique.

TABLE A1 Parameters of the SVCJ model in the benchmark scenarios.

Parameter	Base case	Crisis
κ	1.1521	1.4333
θ	0.3437	0.3779
σ	0.6772	0.9892
ρ	−0.5882	−0.6993
V_t	0.0845	0.0669
λ	3.2642	0.1876
μ_X	−0.0318	0.0473
σ_X	0.0273	0.2295
μ_y	0.2245	0.3962
ρ_J	−0.0921	−0.6677

Abbreviation: SVCJ, stochastic volatility and contemporaneous jump.

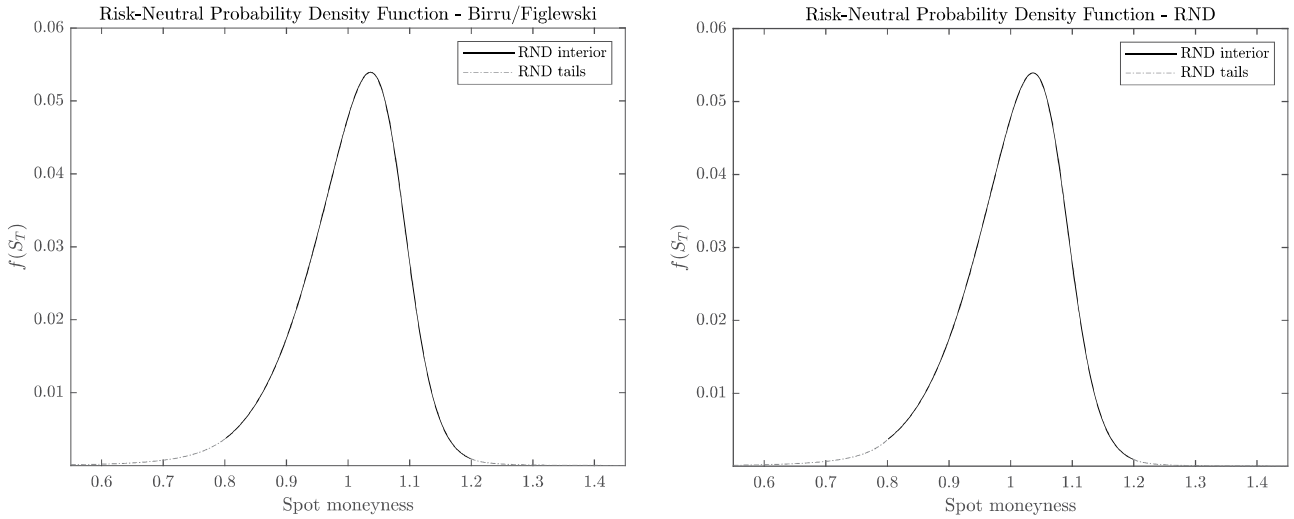

FIGURE A1 Modeled RND tails. The figure plots risk-neutral probability densities with tails modeled according to Birru and Figlewski (2012) (Birru/Figlewski-RND, left panel) and RND-tail extrapolation (RND, right panel). On the basis of benchmark option prices (crisis scenario) generated by the SVCJ model, the risk-neutral probability density inside the spot moneyness range of [0.8, 1.2] ("RND interior") is approximated using finite differences with a fine grid of $\Delta K/S_0 = 0.1\%$, while tails follow from the respective tail-modeling approaches ("RND tails"). RND, risk-neutral return distribution; SVCJ, stochastic volatility and contemporaneous jump.

of [0.8, 1.2] (±20%), we extend the RND implied by available option prices according to both tail-modeling approaches and extract fitted GEV parameters.

Figure A1 shows the RND with tails modeled by both techniques. While tails seem to be equivalent at first glance, Table A2 indicates deviating GEV parameters. In particular, it is striking that the RND-tail extrapolation yields higher values for the shape parameter ξ than the proposed method of Birru and Figlewski (2012). As a consequence, our approach assigns more probability mass to the RND tails which translates into higher option prices and implied volatilities.

Figure A2 plots the extrapolated volatility smiles corresponding to the RNDs depicted in Figure A1. While the higher extrapolated implied volatilities of the RND-tail extrapolation concatenate the smile perfectly, the smaller volatilities of Birru and Figlewski (2012) generate discontinuities at the outermost strikes which are not admissible

TABLE A2 GEV parameters.

	Birru/Figlewski-RND		RND	
	Left tail	**Right tail**	**Left tail**	**Right tail**
μ	98.4106	113.1404	92.1554	114.3723
σ	3.7050	0.1571	1.3680	0.0735
ξ	0.1477	0.5930	0.4102	0.7234

Note: The table shows the fitted location (μ), scale (σ), and shape (ξ) parameters of the generalized extreme value (GEV) distribution resulting from tail modeling according to Birru and Figlewski (2012) and the risk-neutral return distribution (RND) tail extrapolation for the left and the right tail, respectively.

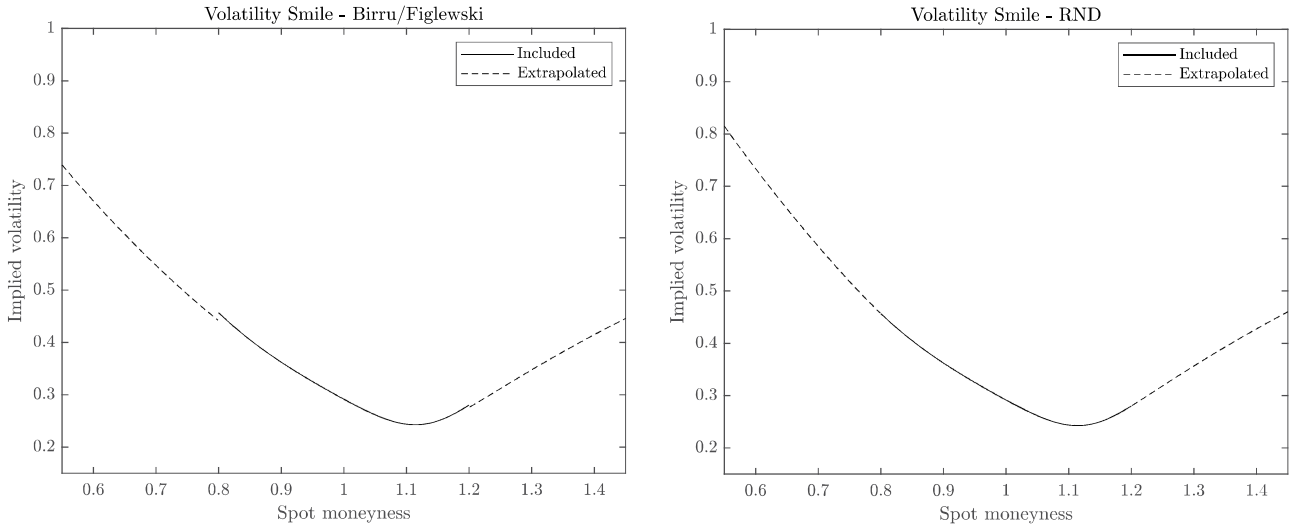

FIGURE A2 Extrapolated volatility smiles. The figure plots extrapolated Black and Scholes (1973) implied volatility smiles resulting from RND-tail modeling according to Birru and Figlewski (2012) (Volatility Smile-Birru/Figlewski, left panel) and the RND-tail extrapolation (Volatility Smile-RND, right panel). Implied volatilities inside the spot moneyness range of [0.8, 1.2] ("Included") result from a dense grid ($\Delta K/S_0 = 0.1\%$) of benchmark option prices (crisis scenario) generated by the SVCJ model detailed in Appendix A.3. Extrapolated implied volatilities follow from RND-tail modeling according to the respective approaches ("Extrapolated"). RND, risk-neutral return distribution; SVCJ, stochastic volatility and contemporaneous jump.

under considerations of no-arbitrage. With respect to $\mathbb{RIX}$ estimates, the higher option prices of the RND-tail extrapolation produce a percentage error of 7.14% only, whereas the error resulting from Birru and Figlewski (2012) amounts to 32.84% due to tail underestimation. Hence, incorporating the martingale property in tail modeling is crucial for smile extrapolation and $\mathbb{RIX}$ estimation.

A.5 | Microstructure noise

See Table A3 and A4.

TABLE A3 Average estimation errors $\mathbb{V}, \mathbb{IV}, \mathbb{RIX}$—Low microstructure noise ($\theta = 1\%$).

	$\mathbb{V}$			$\mathbb{IV}$			$\mathbb{RIX}$		
Observable range	**±25%**	**±20%**	**±15%**	**±25%**	**±20%**	**±15%**	**−25%**	**−20%**	**−15%**
Panel A: Base case scenario									
$\Delta K/S_0 = 1\%$									
EndPoint	1.7012	3.2864	5.9121	1.3159	2.6366	4.9115	8.8509	15.5648	24.8266
	(0.3801)	(0.3839)	(0.4335)	(0.3664)	(0.3673)	(0.4093)	(0.8363)	(0.8944)	(1.0497)
LinReg	0.5183	0.9857	2.0870	0.4419	0.7885	1.7341	2.4604	4.9550	9.5963
	(0.7701)	(1.3968)	(3.3704)	(0.6094)	(1.0190)	(2.3628)	(5.1290)	(8.7475)	(22.8086)
RND	0.4123	0.6915	1.4286	0.3558	0.5650	1.2120	1.7428	3.2716	6.1905
	(0.3304)	(0.5847)	(1.0567)	(0.2825)	(0.4532)	(0.8200)	(1.4922)	(3.2506)	(5.6731)
$\Delta K/S_0 = 2\%$									
EndPoint	1.7170	3.2932	5.9010	1.3314	2.6424	4.8997	8.8637	15.5833	24.8071
	(0.5159)	(0.5332)	(0.6073)	(0.4953)	(0.5142)	(0.5782)	(1.1316)	(1.1621)	(1.3563)
LinReg	0.6942	1.1152	2.1505	0.5966	0.9211	1.7618	3.1795	5.6135	9.7631
	(0.8312)	(2.0274)	(1.9692)	(0.6537)	(1.4344)	(1.5122)	(5.1509)	(14.2492)	(10.4508)
RND	0.5560	0.8201	1.5849	0.4858	0.6770	1.3205	2.2690	3.8600	7.0678
	(0.4622)	(0.7235)	(1.1855)	(0.3870)	(0.5610)	(0.9155)	(2.2955)	(3.9959)	(6.4612)
$\Delta K/S_0 = 5\%$									
EndPoint	1.7478	3.3239	5.9260	1.3869	2.6752	4.9158	8.9049	15.5652	24.9322
	(0.8303)	(0.8479)	(0.8923)	(0.7700)	(0.8257)	(0.8713)	(1.6443)	(1.7054)	(1.6556)
LinReg	0.8359	1.1701	1.8271	0.7695	0.9844	1.5431	3.1140	5.4102	7.8458
	(0.6438)	(0.8974)	(1.2811)	(0.5949)	(0.7387)	(1.0707)	(2.7168)	(4.3407)	(5.6660)
RND	0.7811	1.0207	1.5716	0.7133	0.8731	1.3390	2.7483	4.4782	6.7538
	(0.6009)	(0.7929)	(1.1224)	(0.5469)	(0.6638)	(0.9549)	(2.4890)	(3.7654)	(5.0169)
Panel B: Crisis scenario									
$\Delta K/S_0 = 1\%$									
EndPoint	10.0786	12.8149	16.1582	7.2686	9.5933	12.5665	41.5253	49.0340	56.5959
	(0.3820)	(0.3735)	(0.4062)	(0.3707)	(0.3634)	(0.3941)	(0.6498)	(0.6058)	(0.6360)
LinReg	4.1408	7.1081	10.0933	2.1732	4.8478	7.4814	21.3348	31.3431	40.0307
	(3.1412)	(3.8905)	(5.9449)	(2.0832)	(2.7409)	(3.9039)	(16.0767)	(18.5504)	(28.7684)
RND	3.7016	6.3486	9.2301	2.3872	4.4774	6.8945	17.4203	27.3164	36.1922
	(1.6437)	(2.1569)	(2.3762)	(1.1273)	(1.5495)	(1.8345)	(7.3540)	(9.2560)	(8.4998)
$\Delta K/S_0 = 2\%$									
EndPoint	10.0857	12.8109	16.1429	7.2786	9.5902	12.5513	41.4899	49.0188	56.5702
	(0.5139)	(0.5100)	(0.5656)	(0.5008)	(0.5020)	(0.5539)	(0.8540)	(0.7677)	(0.8174)
LinReg	4.3964	6.9066	9.6942	2.4957	4.6650	7.2166	22.1814	30.7372	37.9981
	(3.5282)	(4.7953)	(3.2668)	(2.5525)	(3.3163)	(2.5085)	(17.1683)	(23.7228)	(11.8234)
RND	3.8484	6.2174	8.9844	2.5062	4.3853	6.7070	17.9930	26.6793	35.2845
	(1.8467)	(2.3825)	(2.7854)	(1.2749)	(1.7273)	(2.1484)	(8.3838)	(9.9900)	(10.0058)

(Continues)

TABLE A3 (Continued)

	$\mathbb{V}$			$\mathbb{IV}$			$\mathbb{RIX}$		
Observable range	**±25%**	**±20%**	**±15%**	**±25%**	**±20%**	**±15%**	**−25%**	**−20%**	**−15%**
$\Delta K/S_0 = 5\%$									
EndPoint	10.0717	12.8128	16.1551	7.2676	9.5973	12.5570	41.4615	48.9577	56.6189
	(0.8215)	(0.7967)	(0.8201)	(0.8169)	(0.7940)	(0.8248)	(1.1681)	(1.0969)	(0.9783)
LinReg	3.7330	6.2552	9.9318	2.1068	3.9585	7.4021	19.3556	28.3534	38.9690
	(2.0138)	(2.4416)	(2.3826)	(1.4431)	(1.9045)	(1.9460)	(8.6599)	(9.1856)	(7.3694)
RND	3.9071	6.1680	9.6527	2.5752	4.3571	7.2166	18.1399	26.2519	37.6687
	(2.0457)	(2.4098)	(2.2106)	(1.4387)	(1.8090)	(1.7746)	(9.1690)	(9.4911)	(7.3631)

Note: The table shows simulation-based averages (1000 runs) of percentage errors $100 \times |\widehat{\mathcal{Y}} - \mathcal{Y}_{\text{dense}}|/\mathcal{Y}_{\text{dense}}$ for $\mathcal{Y} = \mathbb{V}, \mathbb{IV}, \mathbb{RIX}$ using endpoint volatility (EndPoint), linear regression (LinReg), and RND-tail (RND) extrapolation for the base case (Panel A) and crisis scenario (Panel B) with error standard deviation in parentheses. $\mathcal{Y}_{\text{dense}}$ is the respective benchmark computed from the full range of SVCJ OTM option prices $K_{\text{put}}/S_0 \in [0.01, 1]$, $K_{\text{call}}/S_0 \in [1, 1.99]$ ($\mathbb{RIX}$ OTM put options only) using trapezoidal integration over dense grids of strikes with $\Delta K/S_0 = 0.1\%$. Estimates $\widehat{\mathcal{Y}}$ are obtained from randomly perturbed implied volatility smiles $\tilde{\sigma}_{\text{noisy},i} = \tilde{\sigma}_i(1 + 0.01\eta)$, $i = 1, ..., \tilde{N}$, where $\tilde{\sigma}_i$ are Black and Scholes (1973) implied volatilities computed from SVCJ option prices and $\eta \sim \mathcal{N}(0, 1)$. $\widehat{\mathcal{Y}}$ are computed from extrapolated moneyness ranges $[K_{\text{put}}^{\min}/S_0, K_{\text{call}}^{\max}/S_0]$ of [0.75, 1.25] (±25%), [0.8, 1.2] (±20%), and [0.85, 1.15] (±15%) ($\mathbb{RIX}$: OTM put options only) based on cubic spline smoothing (RND: with convexity constraints) of strike grids with $\Delta K/S_0 = 1\%, 2\%, 5\%$.

Abbreviations: OTM, out-of-the-money; RND, risk-neutral return distribution; SVCJ, stochastic volatility and contemporaneous jump.

TABLE A4 Average estimation errors $\mathbb{V}, \mathbb{IV}, \mathbb{RIX}$—High microstructure noise ($\theta = 3\%$).

	$\mathbb{V}$			$\mathbb{IV}$			$\mathbb{RIX}$		
Observable range	**±25%**	**±20%**	**±15%**	**±25%**	**±20%**	**±15%**	**−25%**	**−20%**	**−15%**
Panel A: Base case scenario									
$\Delta K/S_0 = 1\%$									
EndPoint	1.7811	3.2744	5.9319	1.4364	2.6265	4.9255	8.8964	15.5455	24.9815
	(1.0372)	(1.1321)	(1.2582)	(0.9450)	(1.0729)	(1.1942)	(2.4616)	(2.6138)	(2.9313)
LinReg	1.4662	3.9642	4.9204	1.3481	2.8912	3.9267	6.4855	26.7617	27.4641
	(2.3413)	(22.9979)	(20.5245)	(3.3078)	(12.9801)	(13.6706)	(13.4823)	(214.3320)	(174.9337)
RND	1.1256	1.5935	2.6546	0.9933	1.3158	2.1586	4.4013	7.4327	12.5426
	(1.0173)	(1.9345)	(3.7510)	(0.8302)	(1.3569)	(2.5380)	(5.6708)	(13.2398)	(26.5127)
$\Delta K/S_0 = 2\%$									
EndPoint	1.9378	3.2944	5.8813	1.6274	2.6660	4.8721	8.9502	15.6349	24.9766
	(1.2815)	(1.5433)	(1.7813)	(1.1629)	(1.4402)	(1.6974)	(3.3668)	(3.4085)	(3.9027)
LinReg	2.3895	3.4638	4.7285	2.0274	2.7937	3.9262	12.4619	20.6339	23.5885
	(6.6998)	(21.4363)	(10.2468)	(4.2360)	(11.7641)	(7.1874)	(57.7489)	(209.4360)	(77.6022)
RND	1.5312	2.0469	3.4770	1.3589	1.7011	2.7862	6.0691	9.5897	16.9315
	(1.3476)	(2.4093)	(4.8093)	(1.1047)	(1.7103)	(3.2289)	(7.4576)	(16.4170)	(34.2856)
$\Delta K/S_0 = 5\%$									
EndPoint	2.4981	3.5683	5.9276	2.2571	3.0338	4.9014	9.2839	15.6582	25.4695
	(1.8474)	(2.2205)	(2.6359)	(1.7211)	(2.0363)	(2.5499)	(4.5248)	(5.0581)	(4.9632)
LinReg	2.6574	3.1201	3.9295	2.4814	2.7955	3.2886	10.1788	13.6906	17.7699
	(3.2213)	(3.1532)	(4.4319)	(2.6196)	(2.8309)	(3.2895)	(24.0340)	(18.7345)	(26.8616)

TABLE A4 (Continued)

	$\mathbb{V}$			$\mathbb{IV}$			$\mathbb{RIX}$		
Observable range	**±25%**	**±20%**	**±15%**	**±25%**	**±20%**	**±15%**	**−25%**	**−20%**	**−15%**
RND	2.2781	2.7757	3.5752	2.0729	2.3866	2.9950	8.3156	12.1442	16.4955
	(1.8947)	(2.4722)	(3.7677)	(1.6572)	(1.9887)	(2.7489)	(10.2811)	(13.9707)	(24.5172)
Panel B: Crisis Scenario									
$\Delta K/S_0 = 1\%$									
EndPoint	10.1588	12.8446	16.2009	7.3469	9.6234	12.6032	41.5716	49.0304	56.6937
	(1.1290)	(1.0972)	(1.1717)	(1.0981)	(1.0707)	(1.1433)	(1.8899)	(1.7465)	(1.7696)
LinReg	8.7758	15.1291	13.5901	5.3931	9.7540	9.9695	47.1965	78.2070	56.8042
	(62.5362)	(70.2588)	(34.1502)	(28.9650)	(36.3139)	(19.9224)	(440.2742)	(455.7391)	(201.2402)
RND	5.1005	7.3219	10.1877	3.4458	5.2289	7.6042	23.0896	30.8821	39.8171
	(2.5112)	(3.2555)	(4.1925)	(1.8123)	(2.3522)	(2.9795)	(11.0520)	(14.3327)	(18.7555)
$\Delta K/S_0 = 2\%$									
EndPoint	10.1751	12.8503	16.1430	7.3671	9.6273	12.5422	41.4998	49.0391	56.6489
	(1.5225)	(1.5097)	(1.6552)	(1.4849)	(1.4895)	(1.6267)	(2.5150)	(2.2428)	(2.3341)
LinReg	13.3271	15.4141	12.5762	8.2689	9.9186	9.4182	73.4822	83.7409	50.7033
	(66.5418)	(148.9089)	(17.5108)	(32.8188)	(65.7805)	(11.4687)	(450.4826)	(1085.8793)	(91.3701)
RND	5.4608	7.6316	10.2239	3.7321	5.4401	7.5951	24.4190	32.3435	40.2989
	(2.8070)	(3.7293)	(5.0016)	(2.0733)	(2.6680)	(3.5361)	(12.2218)	(16.8888)	(22.6497)
$\Delta K/S_0 = 5\%$									
EndPoint	10.1768	12.8832	16.1581	7.3696	9.6688	12.5250	41.4812	48.9300	56.9045
	(2.4568)	(2.3914)	(2.4630)	(2.4399)	(2.3841)	(2.4865)	(3.4929)	(3.2731)	(2.9312)
LinReg	7.8106	8.2221	10.6668	5.8368	6.0722	7.9760	37.2716	35.4562	41.4469
	(12.4583)	(7.8450)	(5.3707)	(8.2431)	(5.5818)	(4.1756)	(68.9000)	(38.6688)	(20.0501)
RND	5.8443	7.6818	10.0315	4.0681	5.5237	7.4869	26.4100	32.2697	39.2160
	(3.3941)	(4.4302)	(4.4810)	(2.5800)	(3.2397)	(3.5726)	(14.3142)	(19.4865)	(16.6956)

Note: The table shows simulation-based averages (1000 runs) of percentage errors $100 \times |\widehat{\mathcal{Y}} - \mathcal{Y}_{\text{dense}}|/\mathcal{Y}_{\text{dense}}$ for $\mathcal{Y} = \mathbb{V}, \mathbb{IV}, \mathbb{RIX}$ using endpoint volatility (EndPoint), linear regression (LinReg), and RND-tail (RND) extrapolation for the base case (Panel A) and crisis scenario (Panel B) with error standard deviation in parentheses. $\mathcal{Y}_{\text{dense}}$ is the respective benchmark computed from the full range of SVCJ OTM option prices $K_{\text{put}}/S_0 \in [0.01, 1]$, $K_{\text{call}}/S_0 \in [1, 1.99]$ ($\mathbb{RIX}$ OTM put options only) using trapezoidal integration over dense grids of strikes with $\Delta K/S_0 = 0.1\%$. Estimates $\widehat{\mathcal{Y}}$ are obtained from randomly perturbed implied volatility smiles $\tilde{\sigma}_{\text{noisy},i} = \tilde{\sigma}_i(1 + 0.03\eta)$, $i = 1, ..., \tilde{N}$, where $\tilde{\sigma}_i$ are Black and Scholes (1973) implied volatilities computed from SVCJ option prices and $\eta \sim \mathcal{N}(0, 1)$. $\widehat{\mathcal{Y}}$ are computed from extrapolated moneyness ranges $[K_{\text{put}}^{\min}/S_0, K_{\text{call}}^{\max}/S_0]$ of [0.75, 1.25] (±25%), [0.8, 1.2] (±20%), and [0.85, 1.15] (±15%) ($\mathbb{RIX}$: OTM put options only) based on cubic spline smoothing (RND: with convexity constraints) of strike grids with $\Delta K/S_0 = 1\%, 2\%, 5\%$.

Abbreviations: OTM, out-of-the-money; RND, risk-neutral return distribution; SVCJ, stochastic volatility and contemporaneous jump.